



A characterisation study of ignimbrites of Tenerife Island employed as building stone

José A. Valido¹ · José M. Cáceres¹ · Luís Sousa²

Received: 27 January 2023 / Accepted: 6 May 2023 / Published online: 22 May 2023
© The Author(s) 2023

Abstract

The objective of this study is to evaluate the petrophysical properties of four ignimbrites employed as dimension stones. The natural stone under study is produced in Tenerife Island (Spain) under the commercial brand name of Piedra Chasnera and are differentiated according to their chromatic variety into: brown, violet, grey and green. To assess the suitability for feasible applications, it is essential to have a comprehensive knowledge of its properties. In this respect, mineralogical, petrographic and chemical properties were obtained by X-ray diffraction (XRD), polarisation microscopy (POM) and X-ray fluorescence (XRF). According to the procedure described in the standardised methods, apparent density, open porosity, water absorption at atmospheric pressure, water absorption coefficient by capillary and ultrasound propagation velocity were measured. The four variants of ignimbrites were analysed and classified according to the results obtained. It was found that the properties vary depending on the depth of the stratigraphic volcanic level from which the stone is extracted. From the review of the published data, it can be seen that the test results are within the expected values for this lithotype. A comparison was also made with other types of dimensional stones. The correlation analysis shows that there is a high degree of correlation between the physical properties studied.

Keywords Canary islands · Dimension stone · Ignimbrite · Characterization · Physical properties

Introduction

Dimension stone is a natural stone material quarried with the purpose of obtaining blocks or slabs, which can be used for buildings, monuments, paving, furniture, and decorative objects. Since antiquity, dimension stones have been used as building materials, due to their natural beauty and availability, and the diversity of their applications has been increasing ever since (Siegesmund et al. 2018; Sousa et al. 2019; Freire-Lista et al. 2021). As with any other building material, nowadays, dimension stones have to meet the physical and technical requirements demanded by architects

(Siegesmund and Dürrast 2014). The physical properties are of vital importance when natural stones are used for constructing modern structures and buildings. In addition, these properties are directly related to mechanical behaviour and durability, which affect not only the monuments but also the safety of modern buildings (Yarahmadi et al. 2019; Ahmed et al. 2021; Sousa et al. 2021). Therefore, field and laboratory studies are indispensable in investigating the stone quality for purposed structures (Yagiz 2010).

In this context, the number of published studies on natural stone is extensive, leaving evidence that its properties differ according to the type of rock (igneous, sedimentary, metamorphic) and even, for the same type of rock, its physical–mechanical behaviour differs from one lithotype to another. Reviewing the literature and focusing only on research carried out on igneous rocks, numerous works stand out. Yüksek and Demirci (2010) tests different lithotypes from the central region of Turkey, while Kutulus et al. (2012) uses rocks from the north–west region. Pola et al. (2014, 2016) perform a general characterization of the mechanical behaviour of different igneous rocks coming from different areas of Italy, and later from a group of ignimbrites

✉ José A. Valido
jvalidog@ull.es

¹ Dpt. of Industrial Engineering, Escuela Superior de Ingeniería y Tecnología, Instituto Universitario de Materiales y Nanotecnología, University of La Laguna, Campus Anchieta, 38200 San Cristóbal de La Laguna, Tenerife, Spain

² Dpt. of Geology, Geosciences Center (CGeo), University of Trás-os-Montes e Alto Douro, Vila Real, Portugal

from central Mexico. Yang (2015) compares the physical and mechanical characteristics of intact rocks from two regions of South Korea. Schaefer et al. (2015) characterize the igneous rocks of a region in Guatemala and Vieira et al. (2018) obtain the physical and mechanical properties of different samples originating from Madeira (Portugal). It is important to emphasize the work carried out by Engidasew and Abay (2016), who analyse, according to petrographic and physical–mechanical properties, the suitability of the rock in different areas of the city of Addis Ababa (Ethiopia) for potential use as a dimensional stone. Volcanic rock from the Canary Islands has also been studied. González de Vallejo et al. (2006) carry out a complete geomechanical characterisation of the volcanic materials of Tenerife, while Rodríguez-Losada et al.'s (2007a) study the geotechnical properties of intact rock, with the aim of establishing a new classification of volcanic rocks. In this work from Rodríguez-Losada et al. (2007b) the geotechnical characteristics of the welded ignimbrites of the Canary Islands are determined for the first time, associated with two pyroclastic deposits, one of which is the source of the ignimbrites evaluated in this study. In a more recent study, Perucho-Martínez (2018) evaluates the mechanical behaviour of volcanic rocks by laboratory testing of core samples extracted from different locations in the Canary Islands.

These investigations are essential to know the properties of the intact rock, specific to the massif or outcrop; however, to optimise the applications of this resource, when used as a building stone, it is of interest to know its petrophysical properties, as well as its physical–mechanical behaviour.

In this sense, Silva et al. (2002), carried out a lithological and physico-mechanical characterisation of different lithotypes, six commercial specimens, from Madeira and Porto Santo (Portugal). Also from Madeira, specifically from the southwest, comes the basalt characterized by Alves et al. (2017). Sousa et al. (2005) and Sousa (2014) carried out an exhaustive study of nine granites used as dimension stones, quarried in north-western Portugal. In fact, Portugal is one of the world's leading producers of building stones (Carvalho et al. 2018) and numerous authors have investigated the properties of its resources as dimensional stone (Carvalho et al. 2013a, b; Sousa et al. 2016; Santos et al. 2018; Bogdanowitsch et al. 2022). Germinario et al. (2017) obtain the petrophysical and mechanical properties of a set of stones extracted from various areas of northern Italy, historically used as a building material under the commercial name “Zovonite”. Yüsek (2019) determines the mechanical properties of six types of commercial stone, mostly tuff, from Turkey. Mendoza-Chavez et al. (2012) approach their research from an engineering perspective, obtaining the mechanical properties of stones used as pillars in four bridges in southern Mexico.

Although the above-mentioned research is valuable, none of them includes a study and characterization of ignimbrite

as a dimensional stone. With exclusive reference to this lithotype, other similar research has been carried out. For example, the ignimbrites of Turkey have been extensively studied. Öner et al. (2006) obtain the petrographic, geochemical, mechanical and physical properties of a group of ignimbrites, used as building materials, originating from Erzurum. Kekec and Gokay (2009) determine the mechanical properties of four ignimbrites, in addition to a basalt, excavated from Erciyes mountain volcanics in Kayseri, to study the suitability for use in artistic and engineering projects. Along the same lines is the research of Akin et al. (2017), evaluating the physical–mechanical properties of four different types of ignimbrites from the city of Ahlat. A large part of Mexico's architectural heritage is built with ignimbrites, which have been the subject of numerous research studies (Wedekind et al. 2011; López-Doncel et al. 2013, 2016, 2018; Siegesmund et al. 2022).

Studies of ignimbrites from other countries can also be found. Wedekind et al. (2013), studies the deterioration by moisture expansion of a group of ignimbrites from Mexico, Germany and Hungary. In a recently published research, Pötzl et al. (2022), studies the petrography and petrophysics of fifteen ignimbrites, correlating the properties obtained, and including to the statistical and correlation analysis, parameters from other ignimbrites extracted from the literature, from different regions.

Research aimed at studying the physical–mechanical properties of natural stone quarried in the Canary Islands for use as dimension stone, regardless of the lithotype, is practically non-existent. Barbero-Barrera et al. (2019) carry out a thermal, physical and mechanical characterisation of two types of tuffs extracted on the island of Gran Canaria and widely used in traditional construction. Cárdenes et al. (2022) provide information on the physical–mechanical properties of the ignimbrites of Arucas (Gran Canaria), although the aim of their work is really to provide information on the historical significance of this group of ignimbrites and not to study their properties.

Historically, the Canarian aborigines made a rather limited use of stone. They did not know much about the extraction process, nor did they know the metal, so they did not have the right tools for its processing and transformation (Marrero Cabrera 2000). After the conquest of the Canary Islands in the fifteenth century, the first stonemasons arrived from the peninsula to build fortresses, chapels and churches, transmitting their knowledge and implementing the technology available at the time for this sector. It was then that stone, used as a building material, played a fundamental role in the economy and in the development of the industry that emerged after the conquest.

The Canary Islands are one of the most interesting volcanic regions on the planet as practically all possible volcanic processes have taken place there, and a wide spectrum

of useful stones can be found (Hernández-Gutiérrez 2014). This high availability, together with the regulations that favoured the creation of an open quarrying and commercialisation regime (Larraz Mora 1999), contributed to the large number of quarries on the islands, especially in the most inhabited ones (Marrero Cabrera 2000). Initially, the lack of regulation meant that quarries were located almost anywhere. Through successive laws on environment protection and conservation, an extensive network of protected natural areas (natural monuments and reserves, sites of scientific interest, protected landscapes, national parks, etc.) has been defined on the islands; on the island of Tenerife, for instance, these areas represent almost 45% of its surface area. The extractive activity in these protected areas is totally prohibited or restricted, so all of the quarries located in such areas were abandoned. An example of this is the “Piedra de Tindaya”, a grey to light brown trachyte, which extraction was permitted until the “Montaña de Tindaya” was declared a Natural Monument.

Spatial planning legislation limits, for each of the islands, extractive activity to a number of areas (Hernández-Durán 2016). Outside these delimited areas, extractive activity is strictly prohibited, except for those which are made in a handcrafted manner or which are linked to works of public interest. Industry companies study the profitability of exploiting a given resource within in these areas and will

apply or not for an exploitation concession depending on the results obtained in their cost–benefit analysis. There are currently licensed areas without an operating concession. According to Carvalho et al. (2008), the reasons may be very diverse and depend on the following criteria: morphology, structure, fracturing, metamorphism, lithologic characteristics and exploitability. It should be noted that the geomorphological characteristics of the Canary Islands are, in terms of exploitability, one of the most determining factors, since their orography (formed by mountain systems, volcanoes, calderas, ravines, etc.) can condition accessibility increasing the cost of exploiting the resource. On the island of Tenerife, the current planning model sets out thirteen extractive areas (BOC 2011), including the area known as Guama-El Grillo, located in the southern part, where the ignimbrites subject of this study come from.

Figure 1 shows the islands that have active quarries, i.e., authorised quarrying areas with a current mining concession and their location. Only extractive activities where the natural resource exploited is natural stone for use as building stone have been taken into account. It also includes the companies authorised to exploit each of the quarries, as well as the texture and trade name of the stone.

Based on the available literature, this is probably the first work on the petrographic, mineralogical, chemical and physical characterisation of the group of ignimbrites used as

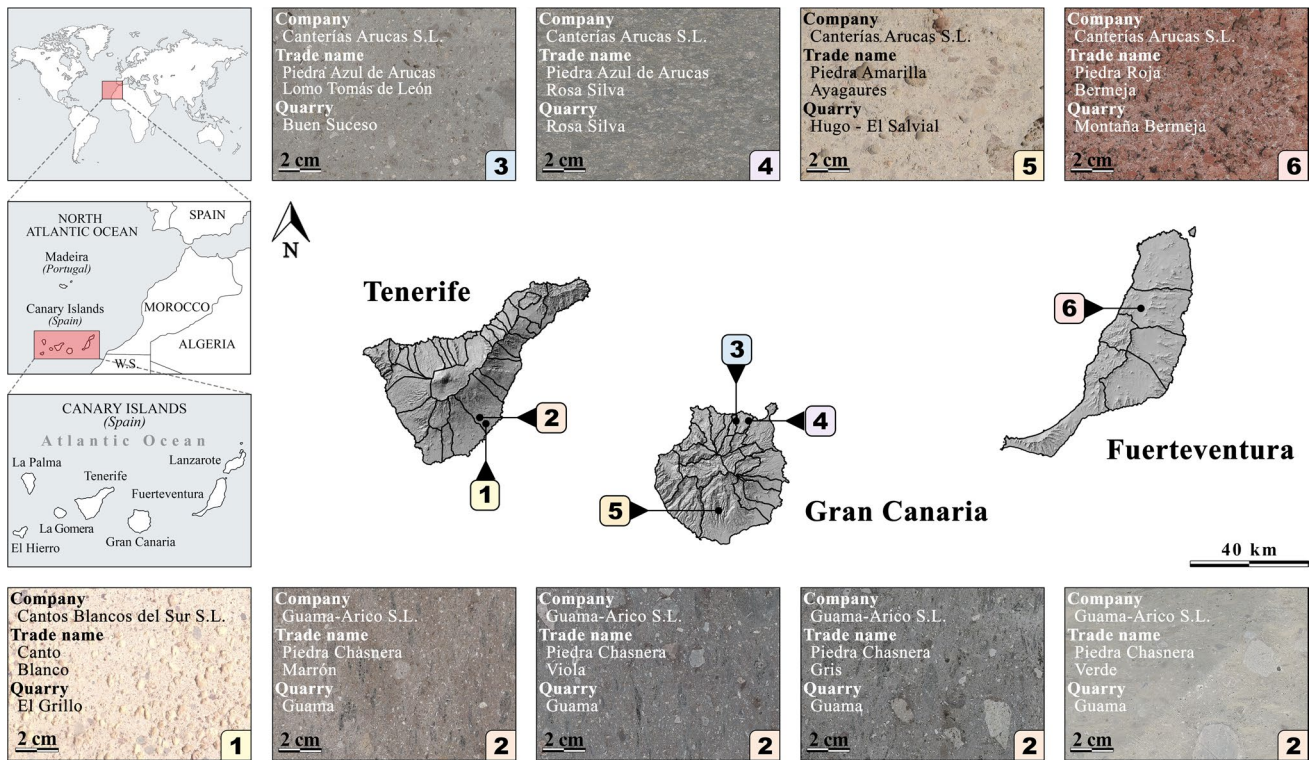


Fig. 1 Islands with active building stone quarries in the Canary Islands

dimension stone under the trade name of “Piedra Chasnera”. Although ignimbrites from other sites have been studied previously, it should be noted that the igneous rocks, and especially ignimbrites, exhibit complex mechanical behaviour due to the large variation in welding, porosity, texture and granulometric characteristics (Pola et al. 2016). The aim of this study is to analyse the behaviour of four chromatic varieties and to contribute to a better scientific knowledge of this lithotype. For this purpose, each variety has been classified according to the most widespread criteria, it has been checked whether the results obtained are related to those reported by other studies, the properties of these ignimbrites were compared with those of other types of stone and a correlation analysis between the different properties was carried out. In addition, this study can enable the scientific community, as well as technicians and engineers, to undertake further research or to adapt their designs and rehabilitation or restoration works, according to the behaviour of this stone.

Materials and methods

Materials

The Canary Islands is an archipelago of volcanic origin located in the Atlantic Ocean and is part of the Macaronesian region with Azores, Cape Verde, Madeira and Salvage Islands. It has a total area of 7501 km², and is made up of seven islands (those with their own administration), of which Tenerife is the largest one (2036 km²). It is also the highest island with the Mount Teide 3718 m altitude, in fact the highest summit elevation in Spain. After Mauna Loa and Mauna Kea in Hawaii, Mount Teide is the third highest volcanic structure and most voluminous in the world. The first scientific theories on the origin of the Canary Islands emerged in the 1970s and several hypotheses have been put forward since then. As far as the island of Tenerife is concerned, the theory most widely accepted by the scientific community suggests that the island was formed from a Central Shield, Roque del Conde (11.9–8.9 Ma) and two later constructions that grew on its flanks, Teno (6.2–5.6 Ma) and Anaga (4.9–3.9 Ma) (Guillou et al. 2004). The eruptive activity of the central shield was followed by a period of calm until the onset of a new eruptive stage marked by the Las Cañadas volcano (3.5 Ma), which developed in three main cycles of activity, each of which involved successive caldera collapses. (Ancochea et al. 1990).

Unlike the basaltic composition of the three shields (Roque del Conde, Teno and Anaga), the magmas of Las Cañadas volcano are characterised by a more evolved composition, mainly phonolites and trachytes rich in dissolved gases (Schwartz-Mesa 2016). This resulted in a series of large explosive Plinian eruptions, producing extensive

pyroclastic deposits on the southern slopes of the island. (Dávila-Harris et al. 2013). This sequence of deposits is known as the “Bandas del Sur Group” and is usually differentiated according to the sector to which they belong, southwest or southeast, into “Bandas del Sur Group in the Adeje Region” or “Bandas del Sur Group in the Abona Region”, respectively (Dávila-Harris 2009). Most of the pyroclastic levels of the “Bandas del Sur Group” are areal projection, pumice fall deposits interspersed with various pyroclastic flows, some with ignimbritic structures, scoria cones, basaltic and phonolitic lavas, epiclastic deposits and paleosols. (Bryan et al. 1998).

The definition of the different stratigraphic levels that make up the “Bandas del Sur Group” varies according to the author. Brown et al. (2003) proposes that the “Bandas del Sur Group” is made up of ten distinct formations, while Edgar et al. (2007) proposes only two major formations, which he further divides into members. However, in most cases, the members defined by Edgar et al. (2007) coincide with the formations proposed by Brown et al. (2003), so it is generally only a change of nomenclature.

The Arico Ignimbrite is one of the units that make up the Arico Formation, being the most recent pyroclastic flow with ignimbritic structure of this formation and the only welded ignimbrite that outcrops in the “Bandas del Sur Group”. (Brown et al. 2003). Its origin is associated with the gravitational or explosive collapse of a dome or lava flow of phonolitic composition (Alonso et al. 1988) and its estimated age is 0.65 Ma (Ancochea et al. 1990). These ignimbrites occur in transitional association with tephritic tuffs. They contain fragments of tephritic pumice slag up to 50 cm, and sporadic nepheline syenite cobbles. Some of the fragments are crushed (fiammes). They are also characterised by loose crystals of feldspar, hauyne and biotite (IGME 2017).

In Fig. 2, which corresponds to the geological map of an area delimited around the quarry, it shows the distribution and location of this lithotype (number 65). In the box above, the island of Tenerife is depicted with the location of the three coats of arms and the area covered by the “Bandas del Sur Group”.

Arico ignimbrite is and has been a popular dimensional stone in the Canary Islands, especially in Tenerife, for many centuries and is often used as a building and ornamental stone. Figure 3 shows some of the most singular constructions made with this stone, being present in many historical buildings, such as, for example, in the main church of the village of Arico, from the seventeenth century (Fig. 3c) or in more modern works as the Plaza de San Pedro, in the village of El Sauzal (Fig. 3j).

The commercialisation and extraction of these ignimbrites is carried by the company Guama-Arico S.L., under the trade name of Piedra Chasnera. According to the colour, four varieties are distinguished as: brown (MA), violet (VA),

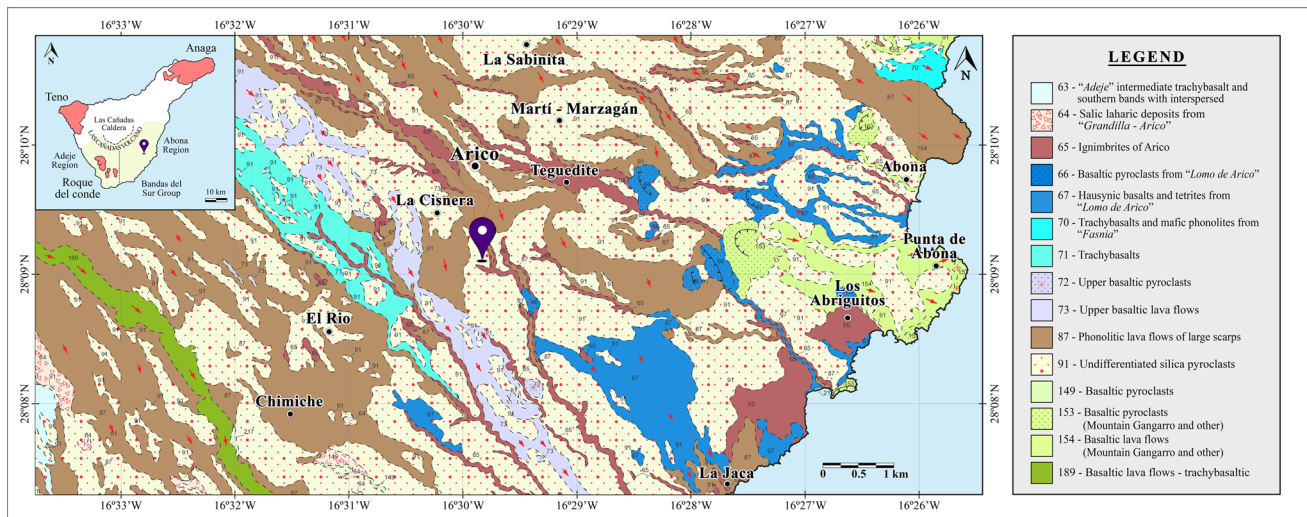


Fig. 2 Geological map with the distribution of the different geological units, the location of the quarry and the population centres (IGME 2007)

grey (GA) and green (VB). The different chromatic varieties of the stone are obtained according to the depth of the excavation, with the brown (MA) variety being the shallowest and the green (VB) variety the deepest. All ignimbrite samples used in this research come from this quarry, located in the municipality of Arico. The coordinates and geographical origin of these ignimbrites are given in Fig. 4a. The quarry currently has three quarrying faces. In Fig. 4b, it can be seen face number 2 on the right side of the picture, which runs along the hillside of the gully, while on the left side of the picture is face number 3, upstream of the channel. In Fig. 4c, it is shown a transition from green (upper zone) to grey colour (lower zone) in the same stone block.

Methods

In the present work, two principal experimental studies can be distinguished. First, a lithological characterisation, with petrographic analysis (polarized microscopy), chemical analysis by X-Ray Fluorescence (XRF) and mineralogical analysis by X-Ray Diffraction (XRD). Second, a physical characterisation by testing; apparent density, open porosity, water absorption at atmospheric pressure, water absorption coefficient by capillary and ultrasound propagation velocity. The tests were performed according to the guidelines and indications of the corresponding standards, following the described methodology and using the recommended dimensions and number of specimens. According to these indications, some tests must be carried out taking into account the anisotropy planes. Depending on the test direction (Fig. 5), the properties obtained are differentiated into normal (Z-axis) and parallel (X-axis) with respect to these planes. All tests performed have been arranged, so

that the test direction is perpendicular to the X–Y anisotropy plane (Z-axis), with the exception of the ultrasound velocity measurement, which is performed in both directions. The interest in analysing this direction (Z-axis) lies in the fact that this is the preferred arrangement used in its commissioning. As set out in the standards, all the tests were done once the specimens were dried to constant mass (weighting each 24 h until less than $\pm 0.1\%$ variation in mass).

In the petrographic analysis, a thin section was examined, of dimensions of 45×25 mm with a thickness of 0.030 ± 0.005 mm, for each of the samples to identify the stone's minerals, texture and structure, in accordance with the UNE-EN 12407 standard (AENOR 2007a). Using a Leica DM750P optical petrographic microscope with a Flexacam C3 microscope camera, more than two hundred images were taken for each thin section and then composited to get to high-resolution overview of the entire surface.

The X-Ray Fluorescence (XRF) chemical analysis of the pulverized samples were carried out by Activation Laboratories Ltd. (Canada), that has ISO/IEC 17025 and CAN-P-1579 accreditation for mineral analysis. The X-Ray Diffraction (XRD) mineralogical analysis was carried out by SIDIX from SEGAI of La Laguna University with a Panalytical X'Pert equipment for Powder Diffraction (Cu $K\alpha$ radiation). The samples were previously pulverized to particle size below $63 \mu\text{m}$.

The apparent density and open porosity was evaluated based on UNE-EN 1936 standard (AENOR 2007b). Apparent density and open porosity were determined by vacuum absorption of water hydrostatic weighing using a pump vacuum Büchi VAC V-100 with controller of vacuum Büchi

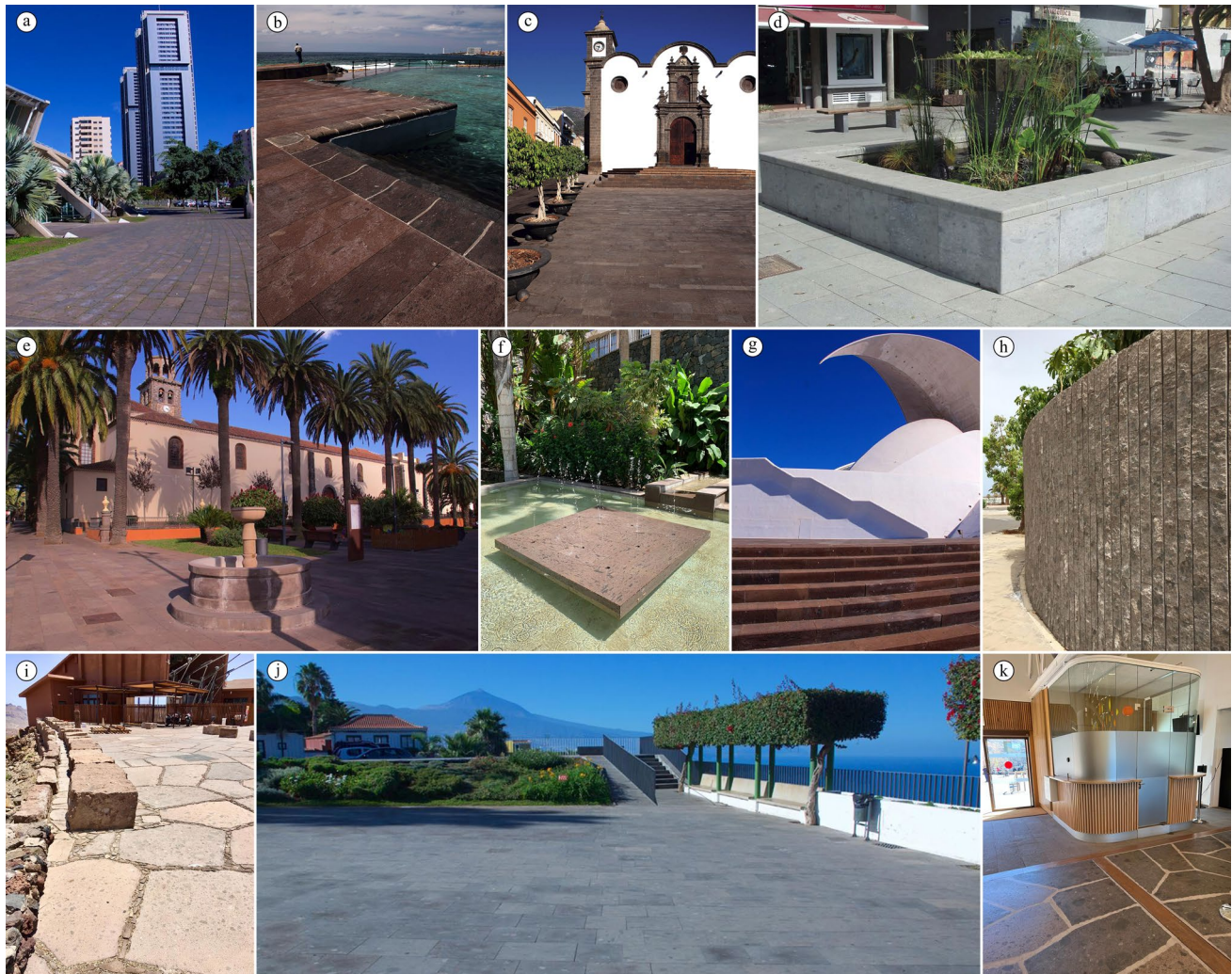


Fig. 3 Examples of buildings with “Piedra Chasnera”. **a** Outside the fairgrounds of Santa Cruz de Tenerife, **b** Natural Pool - La Laguna, **c** San Pedro square - Güímar, **d** Seafont promenade - Los Cristianos, **e** Historic centre of La Laguna (World heritage city - UNESCO 1999), **f** Water source - Hotel “Plantaciones del Sur”, **g** Adan Mar-

tin auditorium outsides - Santa Cruz de Tenerife. **h** Single-family house - Adeje, **i** Teide cable car station square - La Orotava, **j** San Pedro square - El Sauzal and **k** Teide cable car station restaurant - La Orotava (Guama-arico S.L 2021)

I-100 Interface Module. Six cubic specimens (edges measuring 50 mm) were taken:

$$\text{Apparent density (g/cm}^3\text{)} : \quad (1)$$

$$\rho_b = [m_d / (m_s - m_h)] \times \rho_w,$$

$$\text{Open porosity (\%)} : \quad (2)$$

$$p_o = [(m_s - m_d) / (m_s - m_h)] \times 100,$$

where m_d is the dry mass (g), m_s is the saturated mass (g); m_h is the mass when submerged in water (g) and ρ_w is water density (g/cm³).

The water absorption at atmospheric pressure was determined according to the methodology described in UNE-EN 13755 standard (AENOR 2009). The specimens are placed in a tank and water is added gradually at the time intervals described in the standard. After 48 h of total immersion the test specimens are removed from the tank and weighted. Then, the specimens are dipped in water again, repeating the procedure every 24 h, until the difference between two successive weightings does not exceed 0.1%. Six cubic specimens were used (edges measuring 50 mm):

$$\text{Water absorption at atmospheric pressure (\%)} : \quad (3)$$

$$A_b = [(m_d - m_s) / m_s] \times 100,$$



Fig. 4 a Location of the quarry and the extraction company “Guama - Arico” (Google Maps 2021), b Quarry face and c transition between two colours

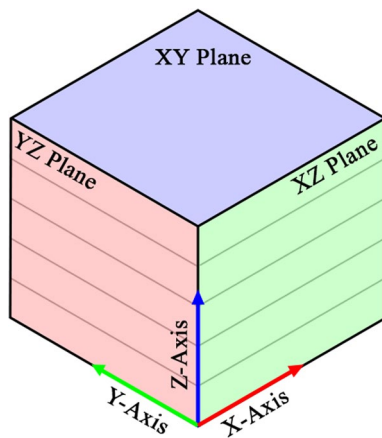


Fig. 5 Test direction (X, Y and Z)

where m_s is the dry mass (g) and m_d is the saturated mass (g).

The water absorption coefficient by capillary was determined following the specifications described in the UNE-EN 1925 standard (AENOR 1999), perpendicular to the anisotropy planes. The specimens are placed on supports in a tank. Water is added until the base of the specimens is partially submerged to a depth of approximately 3 mm. Initially, the samples are weighed at different time intervals, then every 24 h until a constant mass is reached. Once the constant mass has been reached, the mass of water absorbed divided by the area of the submerged base is plotted for each test tube as a function of the square root of time. If the graph obtained can be satisfactorily approximated by two straight lines and the regression coefficient obtained for the first section is greater than 0.90, the water absorption coefficient by capillary is the slope of the regression line. However, if



Fig. 6 Ultrasound propagation velocity test (X-axis direction)

this approximation is not possible, usually for specimens with low absorption, the absorption coefficient is determined by Eq. (4). Six cubic specimens were used (edges measuring 70 mm):

Water absorption coefficient by capillarity ($\text{g/m}^2 \cdot \text{s}^{0.5}$) :

$$C_w = [(m_f - m_d)/A] \times (1/\sqrt{t_f}), \tag{4}$$

where m_f is the final mass (g); m_d is the dry mass (g); A is the submerged base area (m^2) and t_f is the time elapsed from the start of the test until the constant mass is reached (s).

The test to determine the ultrasound P-wave velocity propagation is carried out according to UNE-EN 14579 standard (AENOR 2005). The propagation velocity is obtained as the ratio of the travel length to the time elapsed between the start of the pulse generated at the transmitting transducer and the detection of its arrival at the receiving transducer (Fig. 6). Six specimens of dimensions $300 \times 75 \times 50$ mm were tested. The ultrasound P-wave velocity propagation was determined through a UltraTest GmbH, type BP-7 device, with 29 mm diameter transducers.

The ultrasound velocity is measured, so that the waves propagate perpendicular (Z-axis) and parallel (X-axis) to the planes of anisotropy. In addition to studying the influence of the arrangement of the anisotropy planes on the propagation velocity of the waves, this makes it possible to analyse in future work their relationship with the test direction in obtaining the mechanical properties.

Table 1 summarizes the physical tests performed, identifying the number and size of the specimens used for each test.

Results and discussion

The results obtained for each of the four chromatic varieties object of this study are expressed as the arithmetic mean of the single values of each specimen tested. In addition, the maximum and minimum values of each series are presented, as well as the standard deviation and the coefficient of variation. These

parameters provide relevant information about the degree of dispersion of the data. A comparison is also made with other studies made on ignimbrites, even with other lithotypes.

Petrographic analysis

The lithology is typical of a breccia rock with eutaxitic or flow texture, marked by the orientation of the vitreous fragments in the form of small fiammes (1–3 cm). It contains dispersed angular fragments of trachytic or phonolytic composition (1–5 cm) and abundant feldspar crystals. The ash matrix can present a wide variety of colours. In outcrops they appear in powerful packages of massive rock with few fractures (Hernández-Guitérrez et al. 2015).

Brown sample (MA)

Extrusive igneous rock, with eutaxitic texture. Phenocrysts and lithic fragments are visible, elongated (fiammes) (dashed red line) and rounded (dashed blue line), the latter in smaller

Table 1 Physical tests

Test name	N°	Size (mm)	Standards
Apparent density	6	50×50×50	UNE-EN 1936
Open porosity	6	50×50×50	UNE-EN 1936
Water absorption at atmospheric pressure	6	50×50×50	UNE-EN 13755
Water absorption coefficient by capillarity	6	70×70×70	UNE-EN 1925
Ultrasound propagation velocity	6	300×75×50	UNE-EN 14579

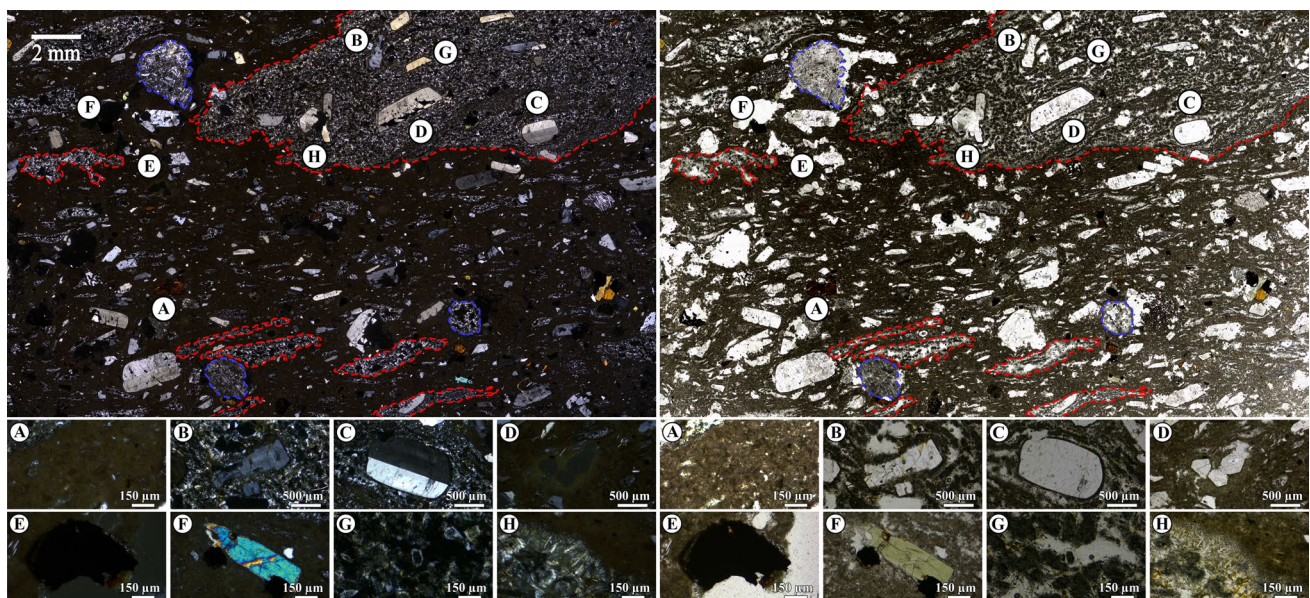


Fig. 7 Full thin section photomicrographs of brown sample (MA) with main minerals displayed (crossed polarized-left; plane polarized-right)

proportions, contained in a cineritic matrix with vitreous characteristics, in which very abundant and dispersed small iron hydroxides are present (A) (Fig. 7). The lithic fragments have a phonolytic/trachytic composition and porphyritic texture with the same phenocrysts found scattered in the cineritic matrix. The most abundant phenocrysts are of anorthoclase (B) and sanidine (C), both unaltered and with a clean appearance. In lesser proportion, sodalite pseudomorphs occur after nepheline, with generally hexagonal sections (D) and opaque minerals, possibly hematite (E), sometimes altered to iron hydroxides. Sporadically, microphenocrysts of augite (F) and phlogopite occur. The aphanitic matrix consists mainly of zoned oligoclase (cloudy core), frequently altered to zeolites, also predominate in the contact between the fiammes and the cineritic matrix (H). Vesicles may also contain zeolites.

Violet sample (VA)

Extrusive igneous rock, with eutaxitic texture. Phenocrysts and highly altered lithic fragments are perfectly distinguished, some of large size (green dashed line). Other are elongated (fiammes; dashed red line), sometimes undulating as consequence of magmatic flow (shaded in red) or rounded (dashed blue line). All these are distributed in a cineritic matrix with vitreous characteristics, which contain abundant small dispersed iron hydroxides (A) (Fig. 8). There is evidence of assimilation of the lithic fragments by the matrix. The lithic fragments have a phonolytic/trachytic composition and porphyritic texture, with the same phenocrysts

found scattered in the cineritic matrix. The most abundant phenocrysts are of anorthoclase (B). In smaller proportions, phenocrysts of sanidine (C), nepheline and microphenocrysts of augite occur. (D). Pseudomorphism of sodalite after nepheline, phlogopite crystals and opaque minerals, probably hematite (E), sometimes altered to hydroxides, are sporadic. In the aphanitic matrix, plagioclase is very sparse, often altered to zeolites (F) and calcite (G). Scattered iron hydroxides (H) are abundant in the zeolites. The vesicular spaces have generally been occupied by zeolites and calcite.

Grey sample (GA)

Extrusive igneous rock, with eutaxitic texture. Phenocrysts and highly altered lithic fragments can be seen in a cineritic matrix with vitreous characteristics and few dispersed iron hydroxides. The lithic fragments can be elongated (fiammes) (dashed red line), sometimes wavy due to magmatic flow (shaded in red) or rounded (dashed blue line) (Fig. 9). Those fragments have a phonolytic/trachytic composition and porphyritic texture with the same phenocrysts found scattered in the cineritic matrix. The predominant phenocrysts are of anorthoclase (A) and sanidine (B), both unaltered and clean appearance. In smaller proportions, sodalite pseudomorphs after nepheline (C) are found. Sporadically, phlogopite (D), augite (E) and opaque minerals, possibly hematite (F), occur. The aphanitic matrix consists mainly of zeolites (G) resulting from the alteration of plagioclase. The vesicles have generally been occupied by zeolites (H).

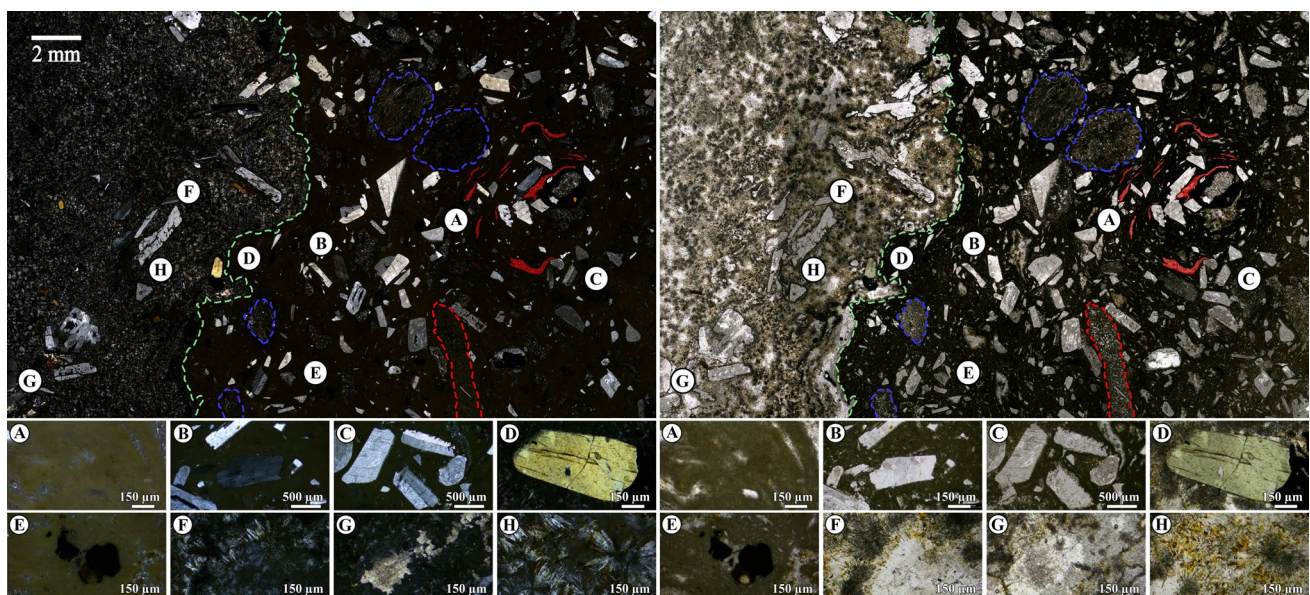


Fig. 8 Full thin section photomicrographs of violet sample (VA) with main minerals displayed (crossed polarized-left; plane polarized-right)

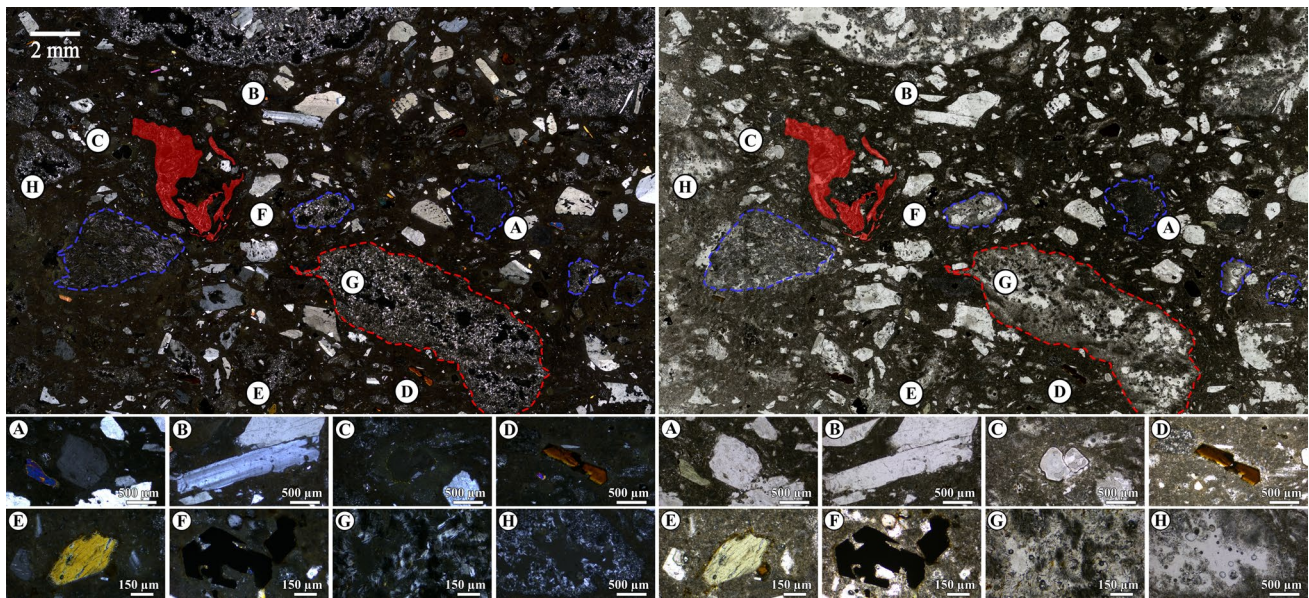


Fig. 9 Full thin section photomicrographs of grey sample (GA) with main minerals displayed (crossed polarized-left; plane polarized-right)

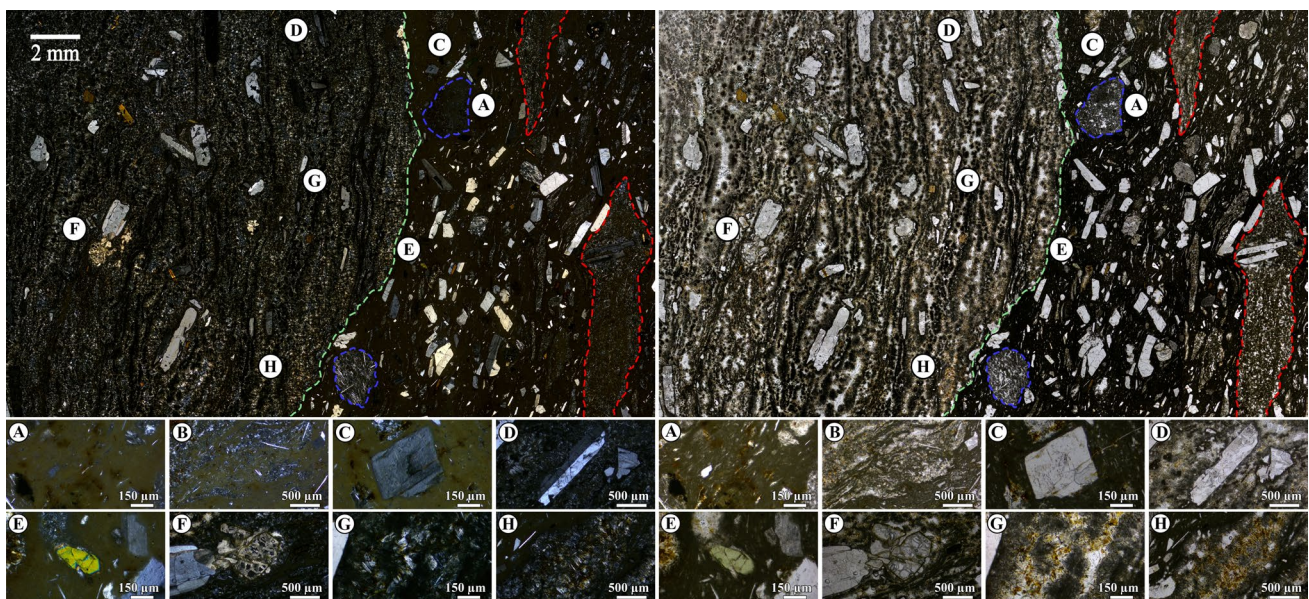


Fig. 10 Full thin section photomicrographs of green sample (VB) with main minerals displayed (crossed polarized-left; plane polarized-right)

Green sample (VB)

Extrusive igneous rock, with eutaxitic texture. Phenocrysts and very altered lithic fragments, some of them large (dashed green line), elongated and very flattened (fiammes) (dashed blue line), contained in a cineritic matrix with vitreous characteristics, can be seen (Fig. 10). This matrix has scattered small iron hydroxides (A) and evidence of areas,

where it assimilates lithic fragments (B). The lithic fragments have a phonolytic/trachytic composition and porphyritic texture with the same phenocrysts found scattered in the cineritic matrix. Anorthoclase (C) and sanidine (D) are the most abundant crystals. In lesser proportion there are microphenocrysts of augite (E), sporadically pseudomorphs of sodalite after nepheline associated with calcite (F), opaque mineral, while phlogopite crystals are scarce. The aphanitic

Table 2 Major element oxides of ignimbrite samples (oxides are expressed as wt %)

Sample	SiO ₂	Al ₂ O ₃	Fe ₂ O ₃	MnO	MgO	CaO	Na ₂ O	K ₂ O	TiO ₂	P ₂ O ₅	LOI	Sum
MA	61.73	18.48	3.68	0.19	0.78	1.08	8.48	4.58	0.95	0.18	0.43	100.6
VA	58.88	18.19	3.49	0.22	0.77	0.93	6.97	5.08	0.78	0.07	5.02	100.4
GA	59.71	18.11	3.78	0.20	0.82	1.25	7.10	4.67	1.00	0.17	2.93	99.7
VB	60.94	18.59	3.87	0.19	0.79	1.23	8.26	4.55	0.99	0.16	0.30	99.9

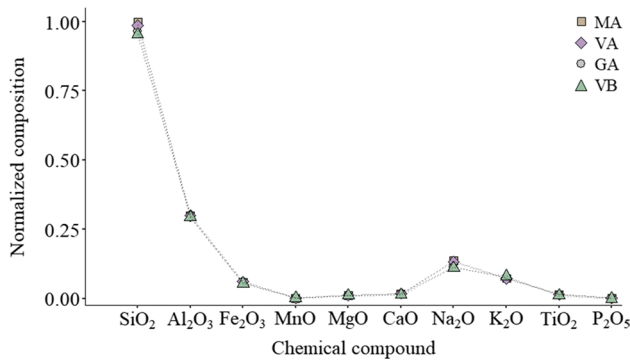


Fig. 11 Normalized chemical composition

matrix is characterised by a low abundance of plagioclase, most of which has been altered to zeolites (G), with abundant iron hydroxides (H). The vesicles are very flattened and occupied by zeolites and calcite.

Chemical analysis: X-ray fluorescence (XRF)

The weight percent of most of the compounds varies from one sample to another by less than 0.5%. In case of manganese oxide (MnO) or magnesium oxide (MgO) is even less than

0.05%. The most notable differences between the maximum and minimum values are for silica oxide (SiO₂) and sodium oxide (Na₂O), with 3.0% and 1.5%, respectively. Table 2 shows the results of the chemical analysis of major elements and the graphic representation in Fig. 11 shows how is similar the chemical composition of the four ignimbrites analysed.

Based on the chemical analysis results, the samples are projected onto the TAS (Bas et al. 1986) and AFM diagrams (Tilley 1960). The boundaries between the alkaline and sub-alkaline series on the TAS diagram and between the calc-alkaline and toleitic series on the AFM diagram correspond to Irvine and Baragar (1971). The location of the samples in these diagrams, according to the geochemistry of the main elements, demonstrates the trachytic composition, belonging to the alkaline series, (Fig. 12a). The calc-alkaline character of the parental magmas is shown in Fig. 12b. The Canary Islands are practically the only region in the world, where ignimbrites are associated with alkaline trachytic–phonolitic magmas (Fúster et al. 1968).

Mineralogical analysis: X-ray diffraction (XRD)

Mineralogical analysis shows that the four ignimbrites studied have a similar mineralogical composition (Fig. 13).

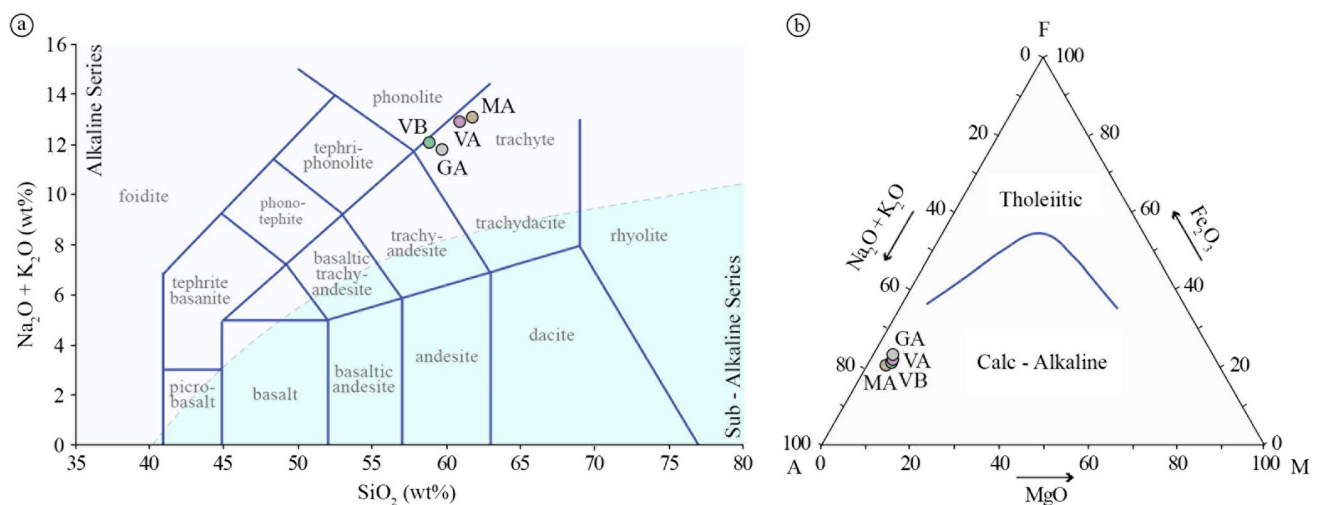


Fig. 12 Chemical classification: **a** Total Alkalis—Silica (TAS) Diagram and **b** relative proportions of the oxides of alkalis (A), iron (F) and magnesium (F) (AFM) Diagram

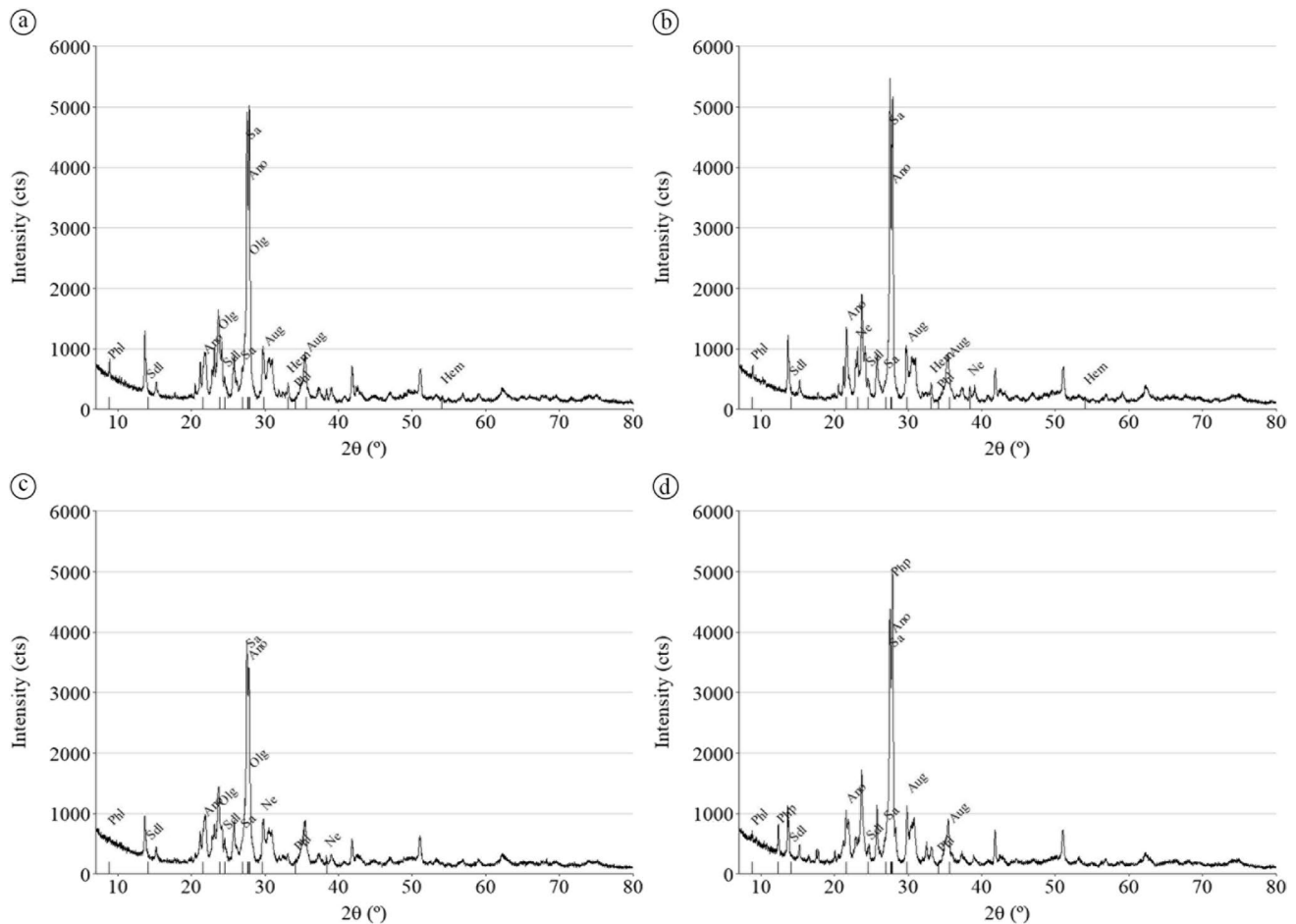


Fig. 13 Diffractograms. **a** Brown (MA), **b** Violet (VA), **c** Grey (GA) and **d** Green (VB). Minerals: Anorthoclase (Ano), Augite (Aug), Hematite (Hem), Nepheline (Ne), Oligoclase (Olg), Phillipsite (Php), Phlogopite (Phl), Sanidine (Sa), Sodalite (Sdl) (Warr 2021)

Anorthoclase (Ano), sanidine (Sa), phlogopite (Phl) and sodalite (Sdl) are minerals common to all samples. Anorthoclase (Ano) and sanidine (Sa) are the most abundant minerals, and phlogopite (Phl) and sodalite (Sdl) the least. In the case of the brown sample (MA) and the grey sample (GA), oligoclase (Olg) is the mineral with the highest occurrence after anorthoclase (Ano) and sanidine (Sa). With exception of grey sample (GA), augite (Aug) is present in all samples,

although the proportion in the brown ignimbrite (MA) is small. Nepheline (Ne) was only detected in the grey sample (GA) and in the violet sample (VA), in both cases in a similar proportion. Hematite (Hem) is another mineral that was only detected in two of the four varieties, brown (MA) and violet (VA). The green ignimbrite (VB) contains phillipsite (Php), a mineral that has only been detected in this chromatic variety.

Table 3 Results of apparent density and open porosity test

	Apparent Density (g/cm ³)				Open Porosity (%)			
	MA	VA	GA	VB	MA	VA	GA	VB
Mean	1.96	2.05	2.18	2.35	25.61	22.10	15.20	2.18
Standard deviation	0.03	0.02	0.05	0.02	1.05	0.71	2.83	0.24
Minimum value	1.93	2.03	2.09	2.30	24.09	21.11	12.06	1.96
Maximum value	2.00	2.08	2.22	2.37	26.75	22.95	20.07	2.61
Coef. of variation	0.01	0.01	0.02	0.01	0.04	0.03	0.19	0.11

Apparent density and open porosity

The results for these tests are shown in Table 3. Small differences can be observed in apparent density, which are more significant or noticeable with respect to open porosity. The green sample (VB) presents the highest apparent density, 2.35 g/cm³, and a really low open porosity with respect to the rest of the samples, at 2.18% as opposed to 15.2%, for the grey sample (GA), which is the next sample with the lowest porosity. It is important to highlight the low variability of the results obtained for apparent density, at a maximum of 2.2%, given for the grey sample (GA). Regarding the open porosity, dispersion varies from only 3% for violet sample (VA), to 19% for the grey sample (GA).

In agreement with to the classification by Anon (1979) for the apparent density of the samples, the grey (GA), brown (MA) and violet (VA) variants belong to class 2

(1.80–2.20 g/cm³), with low densities ranging from 1.96 to 2.18 g/cm³, while the green sample (VB) belongs to class 3 (2.20–2.55 g/cm³). The difference between the green sample (VB) and the rest is even more noticeable in the classification according to open porosity. The green sample (VB) has a low porosity, between 1 and 5% (class 4), while the rest of the samples correspond to class 2 (15–30%). Figure 14 shows graphically the classification of the four ignimbrite variants studied, according to their apparent density and open porosity.

Previous studies by other authors have found that the apparent density of ignimbrites varies between 1.45 and 2.93 g/cm³. Therefore, the apparent density values obtained (between 1.96 and 2.35 g/cm³) are within the expected range for this lithotype. In general terms, the densities of the studied samples are lower than most of the stone types shown in Table 4, practically all the sedimentary and metamorphic

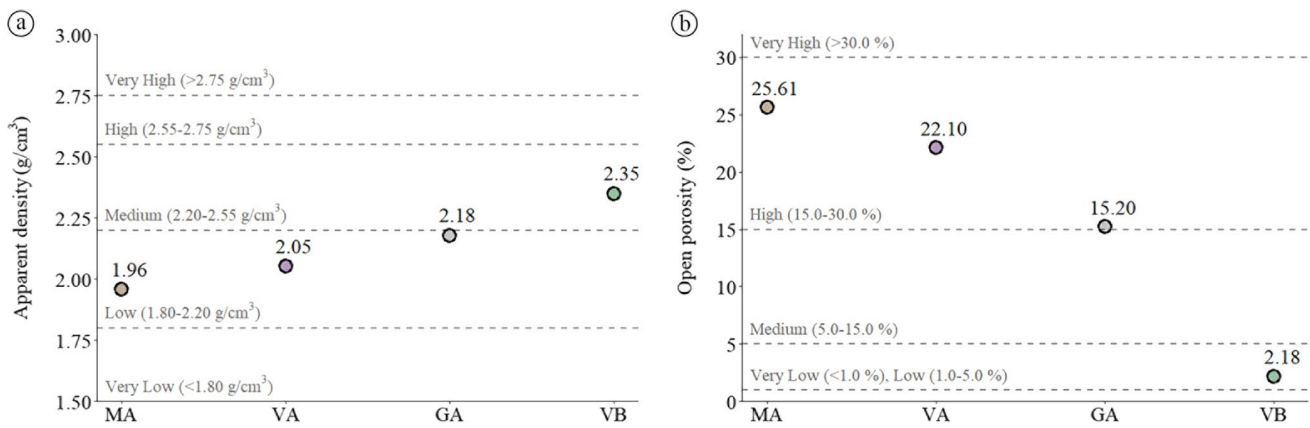


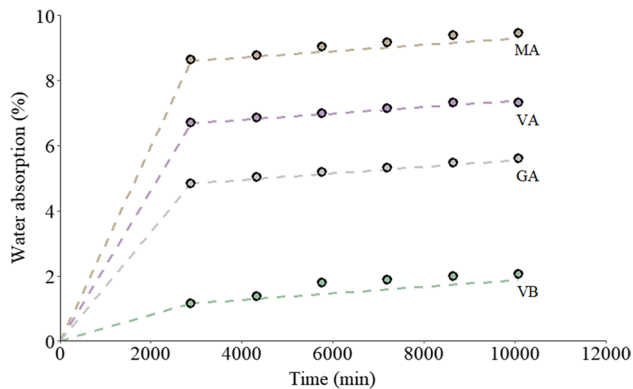
Fig. 14 Classifications of samples according to Anon (1979) by mean values: **a** apparent density and **b** open porosity

Table 4 Apparent density and open porosity of various stones

Rock type	Stone	Apparent density (g/cm ³)	Open porosity (%)	References
Igneous	Basalt	[1.72–3.10]	[0.60–22.80]	Karakuş and Akatay (2013), Engidasew (2014), Vieira et al. (2018)
	Ignimbrite	[1.45–2.91]	[1.37–53.08]	Kecec and Gokay (2009), Engidasew and Asmelash (2016), Martínez-Martínez et al. (2018)
	Trachyte	[2.24–2.46]	[7.67–14.04]	Germinario et al. (2017)
	Trachyandesite	[2.64–2.67]	[1.50–3.90]	Vieira et al. (2018)
	Rhyolite	[2.38–2.81]	[4.46–8.41]	Engidasew and Asmelash (2016)
	Granite	[2.67–2.77]	[0.12–3.72]	Sousa et al. (2005), Karaca et al. (2012); Ozcelik and Ozguven (2014)
	Tuff	[1.35–2.20]	[15.03–47.20]	Engidasew and Asmelash (2016), Vieira et al. (2018), Yüksek (2019)
Sedimentary	Limestone	[2.42–2.76]	[0.25–8.67]	Karaca et al. (2012), Ozcelik and Ozguven (2014), Sarıışık et al. (2016)
	Sandstone	[2.03–2.53]	[6.29–25.57]	Siegesmund and Dürrast (2014)
	Travertine	[2.35–2.56]	[1.17–6.08]	Karaca et al. (2012), Sarıışık et al. (2016)
Metamorphic	Gneis	[2.64–2.96]	[0.16–1.63]	Dias Filho et al. (2014), Siegesmund and Dürrast (2014)
	Marble	[2.65–2.95]	[0.12–1.37]	Karaca et al. (2012), Sarıışık et al. (2016), Navarro et al. (2018)
	Schist	[2.51–2.88]	[0.40–10.00]	Carvalho et al. (2013a, b), Barros et al. (2014)

Table 5 Results from water absorption at atmospheric pressure test

	Water absorption at atmospheric pressure (%)			
	MA	VA	GA	VB
Mean	9.46	7.32	5.60	2.05
Standard deviation	0.32	0.72	0.65	0.48
Minimum value	9.13	6.23	4.51	1.70
Maximum value	9.92	8.30	6.22	2.94
Coef. of variation	0.03	0.10	0.12	0.23

**Fig. 15** Temporal variation of absorption

rocks present higher densities and even within the igneous rocks only the basalts and tuffs present densities in the range of the studied ignimbrites (Table 5).

Similarly, the open porosity values obtained (between 2.18 and 25.61%) are also within the expected range from the literature (1.37 and 53.08%). In this case, it is worth highlighting the great variation of this lithotype, being

ignimbrites the stone with the widest range of porosity. The brown (MA), grey (GA) and violet (VA) samples show porosities similar to some basalts, tuffs or sandstones. The porosity of the green sample (VB), although it could also belong to the basalt group, is more similar to trachyandesite, granite, limestone or travertine.

Water absorption at atmospheric pressure

The absorption of water at atmospheric pressure is strongly conditioned by porosity. Following this pattern, the green sample (VB) presents the lowest absorption, at 2.05%, while the brown sample (MA) present the highest, at 9.46%. Dispersion of results varies between 3 and 23%, corresponding to the brown sample (MA) and the green sample (VB), respectively.

In terms of the time needed to reach saturation, there was no difference. All samples stabilised their saturated mass at the same time, 10080 min (7 days) after starting the test. The greater or lesser capacity to absorb of the samples is latent in the first 2880 min (48 h) and it is in this period that the samples show different absorption rates and which establishes the outcome of the results. After this period the absorption capacity of all samples is similar. This can be seen in Fig. 15 analysing the slopes of the lines, which represent an approximate adjustment of the water absorption of each sample during the course of the test.

The ignimbrite samples in this study have a water absorption values (2.05–9.46%) within the range of data reported by other authors for this lithotype (0.49–12.61%). The water absorption obtained in the green sample (VB) resembles that of some basalts, trachytes and rhyolites, and even some limestones, travertines and schists. However, the grey (GA), brown (MA) and violet (VA) samples

Table 6 Water absorption at atmospheric pressure of various stones

Rock type	Stone	Water absorption (%)	References
Igneous	Basalt	[0.20–9.10]	Engidasew (2014), Moon (2014), Vieira et al. (2018)
	Ignimbrite	[0.49–12.61]	Engidasew (2014), Engidasew and Asmelash (2016)
	Trachyte	[2.10–4.79]	Germinario et al. (2017)
	Trachyandesite	[0.40–1.40]	Vieira et al. (2018)
	Rhyolite	[1.60–3.33]	Engidasew and Asmelash (2016)
	Granite	[0.24–1.72]	Ozcelik and Ozguven (2014), Mustafa et al. (2015)
	Tuff	[6.81–25.18]	Engidasew and Asmelash (2016), Vieira et al. (2018), Yükksek (2019)
Sedimentary	Limestone	[0.14–2.06]	Bayram (2012), Sarıışık et al. (2016)
	Sandstone	[3.20–20.40]	Siegesmund and Dürrast (2014)
	Travertine	[1.42–6.54]	Sarıışık et al. (2016)
Metamorphic	Gneis	[0.39–0.92]	Dias Filho et al. (2014), Ademila (2019)
	Marble	[0.10–0.96]	Mustafa et al. (2015), Sarıışık et al. (2016), Navarro et al. (2018)
	Schist	[0.20–3.55]	Carvalho et al. (2013a, b), Barros et al. (2014), Mustafa et al. (2015)

Table 7 Results from water absorption coefficient by capillarity test

	Water absorption coefficient by capillarity ($\text{g}/\text{m}^2 \text{s}^{0.5}$)			
	MA	VA	GA	VB
Mean	136.64	108.29	24.11	4.30
Standard Deviation	14.87	10.32	1.93	0.70
Minimum Value	155.05	124.81	26.94	5.48
Maximum Value	121.32	97.11	22.78	3.58
Coef. of Variation	0.11	0.10	0.08	0.16

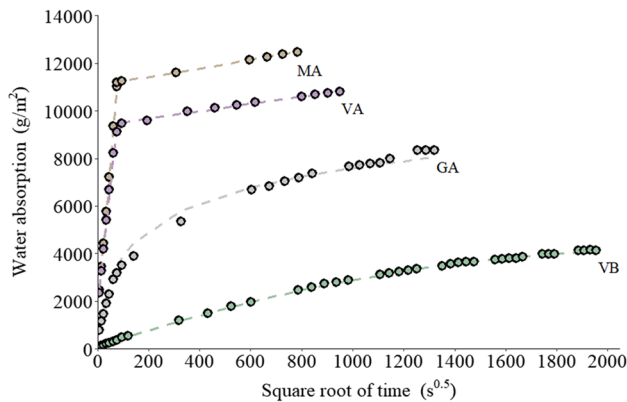


Fig. 16 Mass of water absorbed as a function of the square root of time

barely share absorption with some basalts and tuffs, with absorptions higher than most of the igneous, metamorphic and sedimentary rocks (with the exception of sandstone), as it is shown in Table 6.

Water absorption coefficient by capillarity

The behaviour of the samples against capillary water absorption is similar to that obtained for water absorption at atmospheric pressure. The brown sample (MA), with a capillarity coefficient of $136.64 \text{ g}/\text{m}^2 \text{ s}^{0.5}$ and the green sample (VB), with a capillarity coefficient of $4.30 \text{ g}/\text{m}^2 \text{ s}^{0.5}$ are, respectively, the samples with the highest and lowest capillary absorption capacity. In this test the large difference between these two chromatic varieties also stands out. The violet sample (VA) has an absorption coefficient close to the brown sample (MA), while the grey sample (GA) is close to the green sample (VB), with a difference of 20–25 $\text{g}/\text{m}^2 \text{ s}^{0.5}$ in both cases. The coefficient of variation obtained for all varieties is around 10%, except for the green sample (VB) which shows a dispersion of slightly more than 15% (Table 7). In which two straight sections are clearly identified. In this case, the coefficient of capillary water absorption is determined by the slope of the straight line of the first section. However, for the

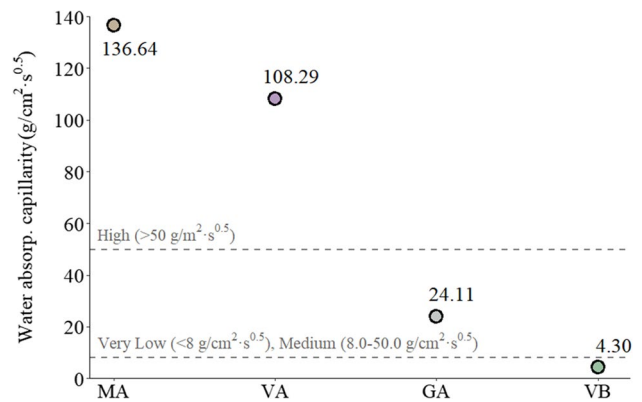


Fig. 17 Classifications of samples according to Snethlage (2005) by mean values water absorption coefficient by capillarity

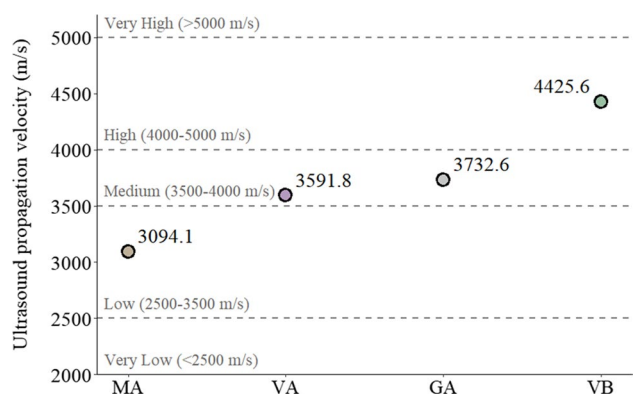


Fig. 18 Classifications of samples according to Anon (1979) by mean values ultrasound propagation velocity

grey (GA) and green (VB) samples, it is not possible to approximate the obtained curve to two straight lines, so the capillary water absorption coefficient is determined by Eq. 4. Figure 16 shows the curves obtained the mean absorption values of the six specimens tested for each of the varieties. The dashed line represents the adjustment made.

The range of the capillary absorption coefficient of the ignimbrites studied ($4.30\text{--}136.64 \text{ g}/\text{m}^2 \text{ s}^{0.5}$) is within the range of data reported by other authors for this lithotype ($0.67\text{--}312.00 \text{ g}/\text{m}^2 \text{ s}^{0.5}$). Most of the stone types listed in Table 8 have a large difference between the maximum and minimum values of the capillary absorption coefficient values. This means that the capillary water absorption coefficients of the ignimbrites studied, independently of the chromatic variety, are also within the range of the rhyolites, limestones, sandstones, travertines and marbles. Even the green sample (VB) presents a capillary water absorption that could practically be associated with all the stone types listed in Table 8, except for the trachyandesites and tuffs. The grey

Table 8 Water absorption coefficient by capillarity of various stones

Rock type	Stone	Water absorp. capillarity (g/m ² s ^{0.5})	References
Igneous	Basalt	[1.01–6.50]	Graue et al. (2011), Engidasew (2014), İnce et al. (2021)
	Ignimbrite	[0.67–312.00]	Pola et al. (2016), Martínez-Martínez et al. (2018), Bustamante et al. (2021)
	Trachyte	[3.31–17.83]	Graue et al. (2011), Germinario et al. (2017), Oliveira (2017)
	Trachyandesite	[104.95–417.06]	İnce (2021)
	Rhyolite	[3.36–579.36]	Engidasew (2014), İnce (2021)
	Granite	[0.50–43.33]	Rivas et al. (2000), Vázquez et al. (2010), Ribeiro (2013)
	Tuff	[8.33–847.26]	Cueto et al. (2018), Ünal and Altunok (2019), Pötzl et al. (2022)
Sedimentary	Limestone	[0.88–293.95]	Buj and Gisbert (2010), Anania et al. (2012), Rodríguez Pérez et al. (2021)
	Sandstone	[0.64–671.00]	Benavente et al. (2007), Franzini et al. (2007), Cnudde et al. (2008)
	Travertine	[0.98–130.00]	Sengun et al. (2015), Benavente et al. (2018), Çelik and İbrahimoglu (2021)
Metamorphic	Gneiss	[-]	
	Marble	[0.07–425.22]	Ozguven and Ozcelik (2013), Navarro et al. (2018), İnce et al. (2021)
	Schist	[1.70–53.21]	Barros et al. (2014), Barroso et al. (2020)

Table 9 Results from ultrasound propagation velocity test (mean values of the two X and Z directions)

	Ultrasound propagation velocity (m/s)			
	MA	VA	GA	VB
Mean	3094.1	3591.8	3732.6	4425.6
Standard deviation	85.2	92.7	137.7	59.8
Minimum value	2970.9	3475.5	3536.7	4356.3
Maximum value	3188.7	3706.8	3965.6	4530.5
Coef. of variation	0.03	0.03	0.04	0.01

sample (GA) also shares absorption with many stone types, in fact, it is only outside the absorption range of basalts, trachytes and trachyandesites.

According to the classification proposed by Sneath (2005), the green sample (VB), with an absorption coefficient of less than 8.0 g/m² s^{0.5} (0.5 kg/m² h^{0.5}) has a very low capillary absorption, while the brown (MA) and violet (VA) samples, with absorption coefficients in both cases higher than 50 g/m² s^{0.5} (3 kg/m² h^{0.5}), show a high capillary absorption. Finally, according to this classification, the grey sample (GA), with an absorption coefficient of 24.11 g/m² s^{0.5}, has a medium capillary absorption (Fig. 17).

Ultrasound propagation velocity

The wave propagation time was measured considering the anisotropy planes of the samples: parallel (*Y*-axis) and normal (*Z*-axis) direction. The results shown in Table 9 correspond to the mean value of the velocities obtained in both directions, measured in each of the six test specimens. The sample with the highest ultrasound propagation velocity is

the green one (VB) and the lowest correspond to the brown sample (MA). The velocity for the grey sample (GA) is slightly higher than for the violet sample (VA). The low variability of the results is noteworthy, with coefficients of variation below 5%.

According to the Anon (1979) classification, five classes are differentiated in terms ultrasound propagation velocity. The brown sample (MA), with the lowest ultrasound velocity, belongs to a class 2. The grey (GA) and violet (VA) samples are in class 3, with a moderate ultrasound velocity. In addition, the green sample (VB), with the highest ultrasound velocity, corresponds to class 4 (Fig. 18).

The mean velocities for the two test directions (normal and parallel) agree with the results obtained for ignimbrites by other authors for ignimbrites, in the range of 1390–4866 m/s. As it can be seen in Table 10, most of the range of velocities are so wide that the results for the analysed ignimbrites could be attributed to virtually any type of stone. Trachyandesites and rhyolites are an exception, showing higher velocities. Trachytes in particular share velocities with grey (GA), violet (VA) and green (VB) chromatic variants, but not with the brown sample (MA), at 3094.1 m/s.

Table 11 shows the ultrasound propagation velocity obtained for the different samples and test directions.

In the four chromatic varieties studied, the propagation speed is greater if the wave travels in a direction parallel to the plane of anisotropy, with a difference of between 5 and 7%, compared to a normal direction. This confirms that the anisotropic characteristics of the stone directly affect the wave velocity (Fort et al. 2011; Karaman et al. 2015). Figure 19 shows the ultrasonic velocity correlation with the test direction.

The correlation between the two test directions, parallel and normal, is almost perfect, with a determination

Table 10 Ultrasound propagation velocity of various stones

Rock type	Stone	Ultrasound prop. velocity (m/s)	References
Igneous	Basalt	[2539–7015]	Karakuş and Akatay (2013), Engidasew (2014), Teymen and Mengüç (2020)
	Ignimbrite	[1390–4866]	Rodríguez-Losada et al. (2007b), Engidasew (2014), Martínez-Martínez et al. (2018)
	Trachyte	[3420–5200]	Vanorio et al. (2002), Kılıç and Teymen (2008), Novotný et al. (2009)
	Trachyandesite	[4020–4640]	Vanorio et al. (2002), Sariisik (2020)
	Rhyolite	[5000–5987]	Müller et al. (2009), Teymen and Mengüç (2020)
	Granite	[2339–6910]	Tuğrul and Zarif (1999), Sousa et al. (2005), Alonso et al. (2008)
Sedimentary	Tuff	[1150–3170]	Çelik and Aygün (2018), Yüksek (2019), Teymen and Mengüç (2020)
	Limestone	[2232–6570]	Anania et al. (2012), Molina et al. (2013), Teymen and Mengüç (2020)
	Sandstone	[1342–4622]	Sarkar et al. (2012), Molina et al. (2013), Ghobadi and Babazadeh (2015)
	Travertine	[2815–6020]	Molina et al. (2013), Benavente et al. (2018), Çelik and İbrahimoglu (2021)
Metamorphic	Gneiss	[2563–4875]	Sharma et al. (2011), Sarkar et al. (2012)
	Marble	[2820–6560]	Durmeková et al. (2015, Navarro et al. (2018), Teymen and Mengüç (2020)
	Schist	[2242–5952]	Sharma et al. (2011), Yagiz (2011), Barros et al. (2014)

Table 11 Results from ultrasound propagation velocity test

	Ultrasound propagation velocity (m/s)							
	X (Parallel direction)				Z (Normal direction)			
	MA	VA	GA	VB	MA	VA	GA	VB
Mean	3189.3	3693.8	3823.3	4578.4	2998.8	3489.8	3642.0	4272.7
Std. deviation	93.9	56.0	106.4	56.9	87.2	132.5	173.4	82.4
Min. value	3058.1	3610.1	3672.0	4504.5	2883.6	3301.3	3401.4	4174.0
Max. value	3289.5	3759.4	3994.7	4665.6	3105.8	3654.3	3936.5	4395.3
Coef. variation	0.03	0.02	0.03	0.01	0.03	0.04	0.05	0.02

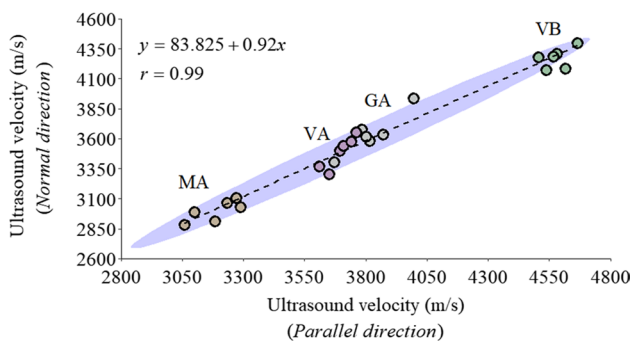


Fig. 19 Relationship between ultrasound propagation velocity parallel and normal direction to the plane of anisotropy

coefficient close to unity. Using the mathematical expression of the adjustment, the value of the ultrasound velocity in a given direction could be obtained from the other with high accuracy.

A summary of the results obtained for the physical properties for the four-ignimbrite variants analysed is presented in Table 12.

Correlation analysis between properties

The regression analyses of the properties obtained in this study are presented and discussed below. A review of the literature shows that there are numerous studies on the correlation between the physical properties of natural stone. The may include several types of stone and/or lithologies (for instance, Barroso et al. (2020)-schist and granite, Kahraman and Yeken (2008)-limestone and travertine or Sarkar et al. (2012)-limestone, sandstone, dolomite, shale, granite, basalt and gneiss), or be dedicated to a single one (Concu et al. (2014) and Parent et al. (2015)—limestone, Azimian and Ajalloeian (2015)-marl or Saldaña et al. (2020)-travertine). The discussion has been based, whenever possible, on those specifically referring to ignimbrites.

Table 12 Summary of physical properties results and classification

	MA	VA	GA	VB
Apparent density [g/cm ³]	1.96±0.03	2.05±0.02	2.18±0.05	2.35±0.02
Class	Low	Low	Low	Medium
Open porosity [%]	25.61±1.05	22.10±0.71	15.20±2.83	2.18±0.24
Class	High	High	High	Very Low
Water absorp. at atmospheric pressure [%]	9.46±0.32	7.32±0.72	5.60±0.65	2.05±0.48
Class	–	–	–	–
Water absorp. coefficient by capillarity [g/m ² ·s ^{0.5}]	136.64±14.87	108.29±10.32	24.11±1.93	4.30±0.70
Class	High	High	Medium	Very Low
Ultrasound propagation velocity [m/s]	3094.1±85.2	3591.8±92.7	3732.6±137.7	4425.6±59.8
Class	Low	Medium	Medium	High

To determine the degree of linear correlation between two properties, the Pearson correlation coefficient “*r*” has been used as a measure, assuming that the variables have a normal distribution. This coefficient ranges from -1 to 1 , for $r < 0$ there is a negative correlation (the two variables are inversely associated), while for $r > 0$, there is a positive correlation (the variables are directly associated). A coefficient $r \approx 0$ indicates that there is no linear relationship between the two variables and an $|r| \approx 1$ means that the variables are almost perfectly correlated. To determine the correlation coefficient, it makes no difference which property is defined as the independent variable (*X*-axis) and which as the dependent variable (*Y*-axis), since in both cases, the result will be the same. The correlation–dispersion diagrams (Fig. 20a–j) are plotted, with the fitting equation for each property pair. The ellipses represent the confidence regions, with a probability range of 85%.

Apparent density and open porosity

The linear relationship between apparent density and open porosity (Fig. 20a) is negative and almost perfect ($r = -0.99$). The negative linear relationship indicates, as expected, that the higher the density, the lower the porosity and vice versa. Similar results have been obtained in other studies; Engidasew and Asmelash (2016) ($r = -0.94$), Barahim et al. (2017) ($r = -0.97$), Colella et al. (2017) ($r = -0.98$). Correlation coefficients above 0.90, derived from the strong correlation between these two properties.

Apparent density and water absorption at atmospheric pressure

Similar results are obtained for correlation analysis between apparent density and water absorption at

atmospheric pressure are obtained. Negative linear correlation and a correlation coefficient close to unity (Fig. 20b). Based on this analysis, it can be concluded that samples with higher density have lower absorption capacity, with absorption capacity increasing as density decreases. The correlation coefficient ($r = -0.96$) is similar to the values found in other studies; Pötzl et al (2022) ($r = -0.92$), Engidasew and Asmelash (2016) ($r = -0.94$). On the other hand, Yasar et al. (2009), made an exponential fit, so it is not directly comparable; however, the coefficient of determination obtained ($R^2 = 0.95$) can be interpreted as meaning that apparent density explains 95% of the variability in water absorption. In any case, the correlation between apparent density and water absorption is high.

Apparent density and capillary water absorption

The linear correlation between apparent density and capillary water absorption is strong, reflecting certain dependence between these two properties, and negative, confirming that samples with lower density have a higher capillary water absorption capacity (Fig. 20c). Barroso et al. (2020) obtained a similar linear correlation coefficient ($r = -0.84$) in their physical characterisation of schist and granite from northwest Portugal. Other authors propose that the best fit between these two properties is not linear but exponential, İnce et al. (2021) ($R^2 = 0.88$), power Rodríguez et al. (2021) ($R^2 = 0.91$) or logarithmic Díçer et al. (2012) ($R^2 = 0.90$). Regardless of the type of adjustment made, the degree of correlation obtained, both in this study and in the literature consulted, confirms that the capillary water absorption coefficient is highly dependent on the density of the sample.

Apparent density and ultrasound velocity

The correlation between apparent density and ultrasound velocity is positive, meaning that the denser the material it passes through, the faster the wave is able to travel, bearing in mind that other factors such as transducer contact, temperature or surface roughness can affect the passage of the wave through the material (Ersoy et al. 2019). The degree of correlation obtained between these two properties is strong ($r=0.95$) (Fig. 20d). This correlation coefficient is similar to those obtained by Azimian and Ajalloeian (2015) ($r=0.96$) or Rahmouni et al. (2013) ($r=0.92$). However, it should be noted that these coefficients are derived from the correlation analysis of the properties of various lithotypes. Few papers in the reviewed literature are focused only on the correlation of these two properties for ignimbrites, standing out the work of Pötzl et al. (2022) in which a moderate correlation is found ($r=0.65$).

Open porosity and water absorption at atmospheric pressure

Open porosity and water absorption at atmospheric pressure show a strong correlation ($r=0.96$) (Fig. 20e). In addition, the correlation is positive, indicating that samples with higher porosity are predisposed to higher absorption capacity. These results do not differ from those reported by other authors; Yasar et al. (2009) ($r=0.98$), Engidasew and Asmelash (2016) ($r=0.99$), even perfect linear correlation, Barahim et al. (2017) ($r=1.00$). It has also been proposed that the best fit between these two properties is exponential (Türkdönmez and Bozcu 2012) or a polynomial of second degree (Murast and Hakki 2016), obtaining in both cases coefficients of determination greater than 0.90.

Open porosity and capillary water absorption

Like water absorption at atmospheric pressure, capillary water absorption shows a strong correlation with open porosity. Similarly, the correlation is positive, so the higher the porosity, the higher the capillary water absorption coefficient (Fig. 20f). The correlation coefficient obtained ($r=0.89$) is lower than that obtained by Çobanoğlu (2015) ($r=0.95$) in his study on the capillary water absorption capacity of travertines used as dimension stone. The difference with the correlation analysis carried out by Barroso et al. (2020), is even greater, as this obtained a linear correlation coefficient close to unity ($r=0.99$). One of the most commonly used settings in the literature to define a power the relationship between these two properties. Mahmutoğlu (2017) ($R^2=0.93$) in his

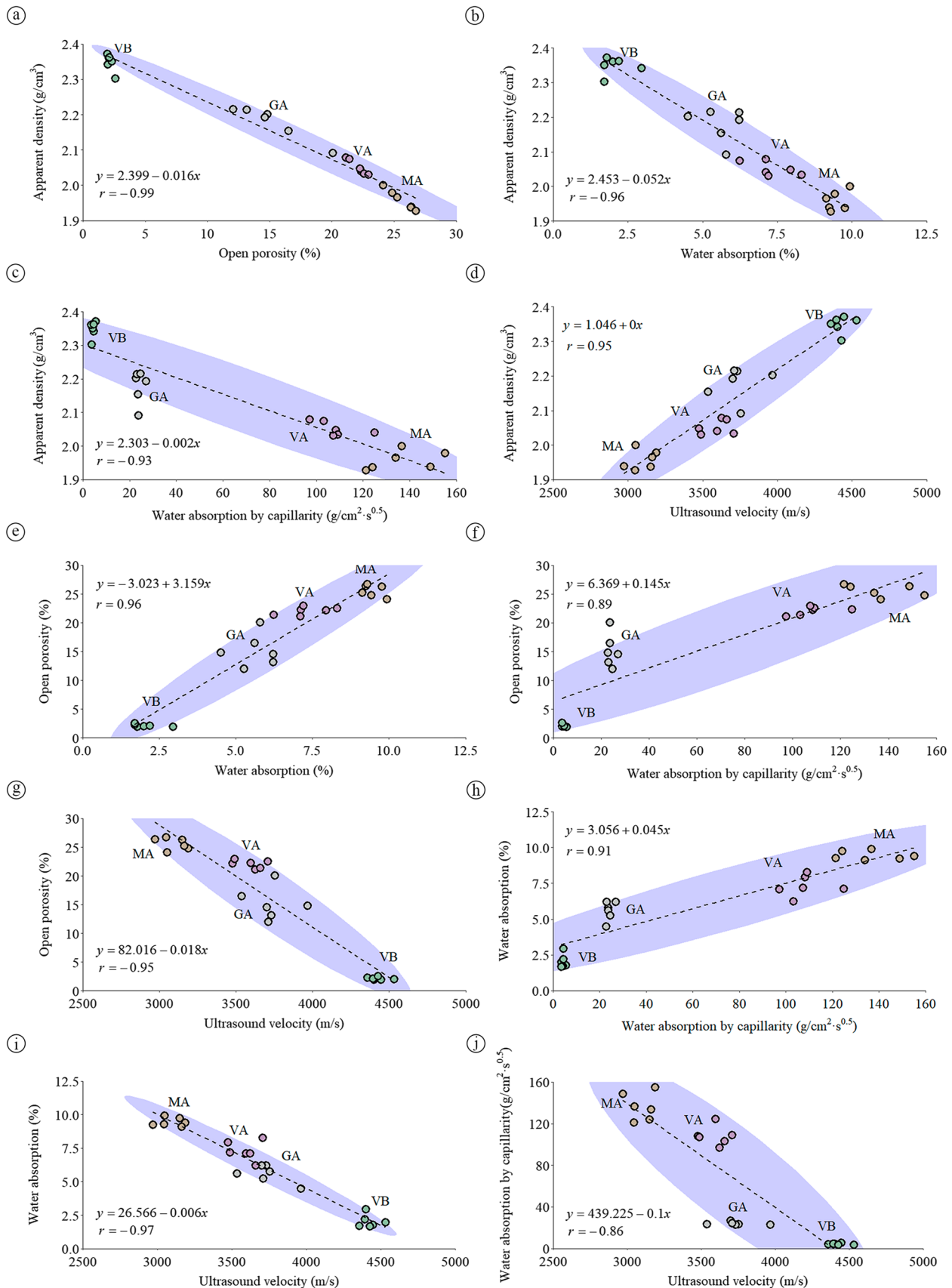
study on marble degradation, İnce et al. (2021) ($R^2=0.88$), in whose study includes different rock types (pyroclastic, volcanic, plutonic and metamorphic) or Rodríguez-Pérez et al. (2021) ($R^2=0.90$) in their research on limestones, are some examples. Others propose an exponential fit (Ünal and Altunok 2019) ($R^2=0.92$).

Open porosity and ultrasound velocity

The correlation between open porosity and ultrasound velocity is also strong ($r=-0.95$), although in this case, the relationship between these two properties is negative (Fig. 20g). Apart from the size and distribution of the pores, the higher the porosity, the more void space the wave encounters on its way between the emitter and the receiver, thus reducing its velocity. In fact, the interpretation of the meaning of the correlation between these two properties is based on the same principle described for apparent density, since density and porosity are closely related. In this case, the comparison with other similar works is inconclusive, while Yüksek (2019) ($r=-0.91$) achieves a strong correlation, Murast and Hakki (2016) propose a second-order polynomial fit, in which only 40% of the porosity variability is explained by the ultrasound velocity, resulting in a weak relationship. In contrast, if a wider variety of lithotypes is taken into account, results analogous to those of the present study are obtained; Engidasew (2014) and Azimian and Ajalloeian (2015) with a coefficient ($r=-0.92$) in both cases, or Rahmouni et al. (2013) ($r=-0.94$).

Water absorption at atmospheric pressure and capillary water absorption

The linear correlation between water absorption at atmospheric pressure and water absorption by capillarity is also strong ($r=0.91$). The relationship between these two properties is positive, so it is to be expected that samples with a higher water absorption capacity at atmospheric pressure will also show a higher willingness to absorb water by capillary action (Fig. 20h). Although in this case the linear fit defines the dependence of these two properties with a high degree of correlation, according to the literature consulted, it is more common to use a potential fit; (İnce et al. 2021) ($R^2=0.92$), (Rodríguez et al. 2021) ($R^2=0.99$) or logarithmic; (Dinçer et al. 2012) ($R^2=0.86$), (Ünal and Altunok 2019) ($R^2=0.92$). Independently, the conclusion is similar, since on the basis of the coefficients determined water absorption at atmospheric pressure is able to explain approximately 90% of the variability of capillary water absorption.



◀**Fig. 20** Regression analysis with trend lines and coefficient r of the different properties obtained in the ignimbrites studied. The blue ellipses predict an 85% probability of the data

Water absorption at atmospheric pressure and ultrasound velocity

After correlation analysis between water absorption at atmospheric pressure and ultrasound velocity, the correlation between these two properties is found to be strong ($r = -0.97$) and negative (Fig. 20i). The fact that water absorption has a strong correlation with density and porosity ($|r| = 0.96$) and that these (density and porosity), in turn, are directly involved in the ultrasound velocity ($|r| = 0.95$) are indications that this result could have been predicted. Yüksek (2019) in an exponential fit also obtained a strong correlation between these two properties, setting that more than 90% of the variability of the ultrasound velocity is explained by water absorption. Similar results with correlation coefficients above 0.90 were also found in other correlation analyses carried out with several lithotypes (Azimian and Ajalloeian 2015; Engidasew 2014).

Capillary water absorption and ultrasound velocity

Finally, capillary water absorption and ultrasound velocity also show a strong linear correlation, although it should be noted that the correlation coefficient ($r = -0.86$) is the lowest of the coefficients obtained in this study. The relationship is negative (Fig. 20j), and it can, therefore, be concluded that samples with higher ultrasonic propagation velocity will have lower capillary water absorption coefficients, and vice versa. This is true, but as mentioned above, the effect of density and porosity on the ultrasound velocity measurement must be taken into account, as these two properties (density and porosity) are indirectly involved in the relationship between capillary water absorption and ultrasound velocity. Vázquez et al. (2010), in their study of granites as ornamental stone, suggest a linear fit between these two properties and conclude that both are strongly correlated ($r = -0.92$). Dinçer et al. (2012) ($R^2 = 0.83$), proposes a logarithmic regression, where ultrasound velocity is able to explain more than 80% of the variability of capillary water absorption, in contrast, Özvan et al. (2015) ($R^2 = 0.46$) although using the same regression model, barely manages to explain 45% of variability. İnce et al. (2021) performs an exponential fit, and achieves a coefficient of determination ($R^2 = 0.68$), although it must be taken into account that their study does not focus on a single lithotype, but collects different rock types.

To conclude this correlation analysis, a matrix with the correlation coefficients obtained between each pair of properties is shown (Fig. 21).

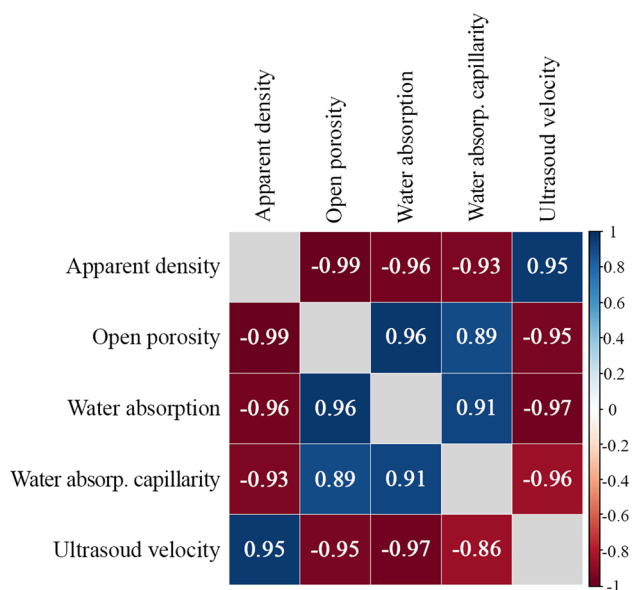


Fig. 21 Correlation matrix of the analysed properties

Confirmation of model

Correlation coefficients close to unity were obtained, meaning a high correlation between the properties analysed. However, it is necessary to assess how significant this correlation is. In other words, if the correlation coefficient is significantly different from zero. The significance of the coefficients can be determined by hypothesis testing, where the null hypothesis is $H_0: r = 0$ and the alternative hypothesis $H_1: r \neq 0$. To reject the null hypothesis, in favour of the alternative, and conclude that the correlation coefficient r is significant, the t value calculated by expression (5) must be greater than the tabulated t value for the confidence level used, 95%. Otherwise, if the calculated t value is lower than the tabulated t value, the null hypothesis is not rejected and the correlation cannot be said to differ significantly from zero. Table 13 shows the results of the t test for the evaluated correlations:

$$t = \frac{r\sqrt{n-2}}{\sqrt{1-r^2}}, \tag{5}$$

where r is the correlation between the two variables, r^2 is the coefficient of determination and n is the sample size.

The calculated t value is in all cases higher than the tabulated t value for a confidence level of 95%; therefore, the null hypothesis can be rejected, concluding that the obtained correlation coefficients r are statistically significant.

Table 13 Results of the *t* test for the evaluated correlation

Properties	<i>r</i>	<i>t</i> calculated	<i>t</i> tabulated
Apparent density and open porosity	0.99	14.04	2.069
Apparent density and water absorption	0.96	6.86	2.069
Apparent density and water absorp. capillarity	0.93	5.06	2.069
Apparent density and ultrasound velocity	0.95	6.08	2.069
Open porosity and water absorption	0.96	6.86	2.069
Open porosity and water absorp. capillarity	0.89	3.90	2.069
Open porosity and ultrasound velocity	0.95	6.08	2.069
Water absorption and water absorp. capillarity	0.91	4.39	2.069
Water absorption and ultrasound velocity	0.97	7.98	2.069
Water absorp. capillarity and ultrasound velocity	0.86	3.37	2.069

Conclusions

Dimensional stone, has been one remarkable resource in local socio-economic development of the Canary Islands (Spain). The lack of initial regulation, together with the high availability and lithological diversity, led to a large-scale exploitation of these resources boom large activity in the exploitation of these resources, with quarries scattered all over the islands. Today, almost all these quarries have been closed, abandoned or have disappeared. On the island of Tenerife, only two quarries are still active, named “Guama” and “El Grillo object of this study on four of the five dimensional stones extracted in those quarries.

Marketed under the trade name of “Piedra Chasnera” it can be differentiated according to its colour into four varieties (brown, violet, grey and green). This type of stone is not only used in modern architecture, but is also present in the island's historical heritage, which is another indicator of the relevance of this study.

The characterization made has provided detailed information on the chemical composition of these four stones, confirming that they are trachytic ignimbrites. From the petrographic/mineralogical analysis it can be concluded that all of them present an eutaxitic texture and a cineritic matrix of a vitreous nature, containing lithic fragments of phonolite/trachytic composition. The brown sample (MA) may owe its colour to the higher amount of hydroxides dispersed in its matrix, which are much more abundant than in the other varieties.

The violet sample (VA) shows greater signs of alteration, although in this case, the hydroxides are mainly located in the lithic fragments, and as a consequence the tone of the sample is not so brown. The vesicles of this sample (VA) have been occupied by secondary minerals, and, therefore, has lower porosity than the brown sample (MA).

The grey sample (GA) is not as altered the previous samples (MA and VA). A greater quantity of iron oxides, not altered to hydroxides stands out, being a possible cause of

the greyish tone of the sample. The vesicles of the lithic fragments are not fully occupied by secondary minerals. However, as the number of lithic fragments is smaller compared to the brown (MA) and violet (VA) samples, the effect on their properties is lower. Furthermore, has a higher degree of compaction, which gives it a higher density and lower porosity.

The green sample (VB) is, according to its petrography, very similar to the violet sample (VA), with the difference that its vesicles and fragments are more elongated and flattened, signs of a higher degree of compaction, and this is confirmed by the properties obtained. It is the sample with the highest proportion of ash, and therefore, its greenish colour is mainly due to this fact.

For all the physical properties analysed the same sort according to the stratigraphic levels is found: brown (MA), violet (VA), grey (GA) and green (VB). The brown (MA) and violet (VA) samples, coming from levels closer to the surface, have very similar physical properties. The results for the grey sample (GA), coming from deeper stratigraphic level, are slightly different from those of MA and VA samples. The green sample (VB), corresponding to the deepest level, shows marked differences respect the other three samples.

The results obtained are in accordance with those reported in the literature for this type of lithology; however, in some cases, VB sample could be attributed to another type of stone. From the correlation analysis carried out, it is concluded that the degree of linear correlation between the different physical properties obtained is very strong, with correlation coefficients equal to or greater than 0.95 in all cases.

The properties obtained in this study, especially porosity and water absorption, can be used as indicators to qualitatively estimate deterioration resistance. The brown ignimbrite (MA) and the violet ignimbrite (VA) are the samples with the highest porosity and water absorption, so they are expected to be the most prone to deterioration. On the other

hand, the grey sample (GA) and especially the green sample (VB) have a lower porosity and absorption, which hinders the penetration of water and other pollutants that may accelerate their degradation, giving these two varieties, in principle, a greater resistance to deterioration.

Future research can be carried out on the basis of this study. The physical properties, many of which are presented here, are closely related to durability, as discussed above, and, therefore, would be perfectly complemented by the analysis of the effects caused by exposure to extreme environments (accelerated ageing tests), this being fundamental given the heritage and cultural value of the works in which these ignimbrites have been used. On the other hand, this study could be extended to include the mechanical properties, which are essential to determine the bearing capacity of this group of ignimbrites and to include new relationships to predict the behaviour of these dimension stones under the stress of a given load.

Acknowledgements We are grateful to the “Servicio de Laboratorios y Calidad de la Construcción del Gobierno de Canarias” for their collaboration in the execution of the tests, to the “Guama-Arico S.L” quarry for providing the necessary samples to carry out this study and to Prof. Dr. Rui Teixeira for his help with the petrographic description.

Author contributions JA Valido: conceptualization, analysis, investigation, methodology, writing, editing, and funding acquisition. JM Caceres: methodology, editing, supervision, review and visualization. Luis Sousa: editing, supervision, review and visualization

Funding Open Access funding provided thanks to the CRUE-CSIC agreement with Springer Nature. The X-Ray Fluorescence tests were financed through the Nuclear Safety Council PR32960 “Radon emission in the volcanic materials of the Canary Islands. Implications for residential infrastructures and public works” project. This study was supported by the “Fundação para a Ciência e a Tecnologia” in the frame of the UIDB/00073/2020 and UIDP/00073/2020 projects of the I&D unit Geosciences Center (CGEO) and by the Ministry of Universities of Spain, through the pre-doctoral contract of the first author (FPU16/05739).

Data availability The data will be available on request by contacting the first author.

Declarations

Conflict of interest The authors have not disclosed any competing interests.

Open Access This article is licensed under a Creative Commons Attribution 4.0 International License, which permits use, sharing, adaptation, distribution and reproduction in any medium or format, as long as you give appropriate credit to the original author(s) and the source, provide a link to the Creative Commons licence, and indicate if changes were made. The images or other third party material in this article are included in the article's Creative Commons licence, unless indicated otherwise in a credit line to the material. If material is not included in the article's Creative Commons licence and your intended use is not permitted by statutory regulation or exceeds the permitted use, you will need to obtain permission directly from the copyright holder. To view a copy of this licence, visit <http://creativecommons.org/licenses/by/4.0/>.

References

- Ademila O (2019) Engineering geological evaluation of some rocks from Akure, southwestern Nigeria as aggregates for concrete and pavement construction. *Geology Geophys Environ* 45:31. <https://doi.org/10.7494/geol.2019.45.1.31>
- AENOR (1999) UNE-EN 1925. Natural stone test methods. Determination of water absorption coefficient by capillarity. Spanish Association for Standardisation and Certification
- AENOR (2005) UNE-EN 14579. Natural stone test methods. Determination of sound speed propagation. Spanish Association for Standardisation and Certification.
- AENOR (2007a) UNE-EN 12407. Natural stone test methods. Petrographic Examination. Spanish Association for Standardisation and Certification.
- AENOR (2007b) UNE-EN 1936. Natural stone test methods. Determination of real density and apparent density, and of total and open porosity. Spanish Association for Standardisation and Certification.
- AENOR (2009) UNE-EN 13755. Natural stone test methods. Determination of water absorption at atmospheric pressure. Spanish Association for Standardisation and Certification
- Ahmed I, Basharat M, Sousa L, Mughal MS (2021) Evaluation of building and dimension stone using physico-mechanical and petrographic properties: A case study from the Kohistan and Ladakh batholith. *Northern Pakistan Environ Earth Sci* 80:759. <https://doi.org/10.1007/s12665-021-10007-y>
- Akın M, Özvan A, Dinçer İ, Topal T (2017) Evaluation of the physico-mechanical parameters affecting the deterioration rate of Ahlat Ignimbrites (Bitlis, Turkey). *Environ Earth Sci* 76:827. <https://doi.org/10.1007/s12665-017-7175-7>
- Alonso JJ, Araña V, Marti J (1988) La Ignimbrita de Arico (Tenerife). Mecanismos de emisión y de emplazamiento. *Rev Soc Geol Esp* 1:15–24
- Alonso FJ, Vázquez P, Esbert RM, Ordaz J (2008) Ornamental granite durability: Evaluation of damage caused by salt crystallization. *Mater Constr* 58:191–201
- Alves R, Faria P, Simão J (2017) Experimental characterization of a Madeira Island basalt traditionally applied in a regional decorative mortar”. *J Build Eng* 13:326–335. <https://doi.org/10.1016/j.jobe.2017.09.004>
- Anania L, Badalà A, Barone G, Belfiore CM, Calabrò C, La Russa MF, Mazzoleni P, Pezzino A (2012) The stones in monumental masonry buildings of the “Val di Noto” area: New data on the relationships between petrographic characters and physical–mechanical properties. *Constr Build Mater* 33:122–132. <https://doi.org/10.1016/j.conbuildmat.2011.12.076>
- Ancochea E, Fuster JM, Ibarrola E, Cendrero A, Coello J, Hernan F, Cantagrel JM, Jamond C (1990) Volcanic evolution of the island of Tenerife (Canary Islands) in the light of new K–Ar Data. *J Volcanol Geotherm* 44:231–249. [https://doi.org/10.1016/0377-0273\(90\)90019-C](https://doi.org/10.1016/0377-0273(90)90019-C)
- Anon (1979) Classification of rocks and soils for engineering geological mapping. Part 1: Rock and soil materials. *Bull Int Assoc Eng Geol* 19:364–371. <https://doi.org/10.1007/BF02600503>
- Azimian A, Ajalloeian R (2015) Empirical correlation of physical and mechanical properties of marly rocks with P-Wave velocity. *Arab J Geosci* 8:2069–2079. <https://doi.org/10.1007/s12517-013-1235-4>
- Barahim AA, Al-Akhaly IA, Shamsan RI (2017) Engineering properties of volcanic tuff from the western part of Yemen. *Sultan Qaboos Univ J Sci* 22:81–88
- Barbero-Barrera MM, Flores-Medina N, Moreno-Fernández E (2019) Thermal, physical and mechanical characterization of volcanic tuff masonries for the restoration of historic buildings. *Mater Constr*. <https://doi.org/10.3989/mc.2019.12917>

- Barros RS, Oliveira DV, Varum H, Alves AS, Camões A (2014) Experimental Characterization of Physical and Mechanical Properties of Schist from Portugal. *Constr Build Mater* 50:617–630. <https://doi.org/10.1016/j.conbuildmat.2013.10.008>
- Barroso CE, Oliveira DV, Ramos LF (2020) Physical and mechanical characterization of vernacular dry stone heritage materials: schist and granite from northwest Portugal. *Constr Build Mater* 259:119705. <https://doi.org/10.1016/j.conbuildmat.2020.119705>
- Bayram F (2012) Predicting mechanical strength loss of natural stones after freeze–thaw in Cold Regions. *Cold Reg Sci Technol* 83–84:98–102. <https://doi.org/10.1016/j.coldregions.2012.07.003>
- Benavente D, Cueto N, Martínez-Martínez J, García del Cura MA, Cañaveras JC (2007) The influence of petrophysical properties on the salt weathering of porous building rocks. *Environ Geol* 52:197–206. <https://doi.org/10.1007/s00254-006-0475-y>
- Benavente D, Martínez-Martínez J, Cueto N, Ordoñez S, García del Cura MA (2018) Impact of salt and frost weathering on the physical and durability properties of travertines and carbonate tufas used as building material. *Environ Earth Sci* 77:1–13. <https://doi.org/10.1007/s12665-018-7339-0>
- BOC (2011) Decreto 56/2011, de 4 de Marzo, por el que se aprueba la Revisión Parcial del Plan Insular de Ordenación de Tenerife (PIOT) para su adaptación a las Directrices de Ordenación General, para la racionalización del Planeamiento Territorial de Desarrollo del PIOT. Boletín Oficial De Canarias 58:5440–5822
- Bogdanowitsch M, Sousa L, Siegesmund S (2022) Building stone quarries: Resource evaluation by block modelling and unmanned aerial photogrammetric surveys. *Environ Earth Sci* 81:16. <https://doi.org/10.1007/s12665-021-10031-y>
- Brown RJ, Barry TL, Branney MJ, Pringle MS, Bryan SE (2003) The quaternary pyroclastic succession of southeast Tenerife, Canary Islands: Explosive eruptions, eelated caldera subsidence, and sector collapse. *Geol Mag* 140:265–288. <https://doi.org/10.1017/S0016756802007252>
- Bryan S, Martí J, Cas R (1998) Stratigraphy of the Bandas del Sur formation: An extracaldera record of quaternary phonolitic explosive eruptions from the Las Cañadas edifice, Tenerife (Canary Islands). *Geol Mag* 135:605–636. <https://doi.org/10.1017/S0016756897001258>
- Buj O, Gisbert J (2010) Influence of Pore Morphology on the durability of sedimentary building stones from Aragon (Spain) subjected to standard salt decay tests. *Environ Earth Sci* 61:1327–1336. <https://doi.org/10.1007/s12665-010-0451-4>
- Bustamante R, Vazquez P, Prendes N (2021) Properties of the Ignimbrites in the Architecture of the Historical Center of Arequipa, Peru. *Appl Sciences* 11:10571–10588. <https://doi.org/10.3390/app112210571>
- Cárdenes V, Cabrera-Guillén D, López-Piñeiro S, Ruiz de Argandoña V, Rubio-Ordóñez A (2022) The historical significance of the welded tuffs from Arucas, Canary Islands. *Geoheritage* 14:1–10. <https://doi.org/10.1007/s12371-022-00680-1>
- Carvalho J, Henriques P, Falé P, Luís G (2008) Decision criteria for the exploration of ornamental-stone deposits: application to the marbles of the portuguese Estremoz anticline. *Int J Rock Mech Min Sci* 45:1306–1319. <https://doi.org/10.1016/j.ijrmm.2008.01.005>
- Carvalho C, Aires S, Noronha F, Casal-Moura A, Farinha-Ramos J (2013a) “Schist” from Trás-Os-Montes and Alto Douro (NE of Portugal): potential use as natural stone. *Key Eng Mater* 548:205–211. <https://doi.org/10.4028/www.scientific.net/kem.548.205>
- Carvalho JMF, Lisboa JV, Moura AC, Carvalho C, Sousa LMO, Leite MM (2013b) Evaluation of the Portuguese ornamental stone resources. *Key Eng Mat* 548:3–9. <https://doi.org/10.4028/www.scientific.net/KEM.548.3>
- Carvalho J, Lopes C, Mateus A, Martins L, Goulão M (2018) Planning the future exploitation of ornamental stones in Portugal using a weighed multi-dimensional approach. *Resour Policy* 59:298–317. <https://doi.org/10.1016/j.resourpol.2018.08.001>
- Çelik MY, Aygün A (2018) The effect of salt crystallization on degradation of volcanic building stones by sodium sulfates and sodium chlorides. *Bull Eng Geol Environ* 78:3509–3529. <https://doi.org/10.1007/S10064-018-1354-Y>
- Çelik MY, İbrahimoglu A (2021) Characterization of travertine stones from Turkey and assessment of their durability to salt crystallization. *J Build Eng* 43:102592. <https://doi.org/10.1016/j.job.2021.102592>
- Cnudde V, Dierick M, Vlassenbroeck J, Masschaele B, Lehmann E, Jacobs P, Van Hoorebeke L (2008) High-speed neutron radiography for monitoring the water absorption by capillarity in porous materials. *Nucl Instrum Methods Phys Res B* 266:155–163. <https://doi.org/10.1016/j.nimb.2007.10.030>
- Çobanoğlu İ (2015) Prediction and identification of capillary water absorption capacity of travertine dimension stone. *Arab J Geosci* 8:10135–10149. <https://doi.org/10.1007/s12517-015-1902-8>
- Colella A, Di Benedetto C, Calcaterra D, Cappelletti P, D’Amore M, Di Martire D, Graziano DF, Papa L, Langella A (2017) The Neapolitan Yellow Tuff: An outstanding example of heterogeneity. *Constr Build Mater* 136:361–373. <https://doi.org/10.1016/j.conbuildmat.2017.01.053>
- Concu G, De Nicolò B, Valdes M (2014) Prediction of building limestone physical and mechanical properties by means of ultrasonic P-wave velocity. *Sci World J*. <https://doi.org/10.1155/2014/508073>
- Cueto N, Vieira de Sousa JF, Fernandes C, Benavente D, Urbani F, Meza R, Santos JP, García del Cura MJ (2018) Water transport in lapilli tuff from Madeira Island, Portugal: Implications on degradation mechanisms and durability. In: *Proceeding of conference 16° Congresso Nacional de Geotecnia, Azores, Portugal, 27–30 May, 2018*.
- Dávila-Harris P (2009) Explosive ocean-island volcanism: the 1.8–0.7 Ma explosive eruption history of Cañadas volcano recorded by the pyroclastic successions around Adeje and Abona, southern Tenerife, Canary Islands. Ph.D. thesis. University of Leicester, Leicester, England
- Dávila-Harris P, Ellis BS, Branney MJ, Carrasco-Núñez G (2013) Lithostratigraphic analysis and geochemistry of a vitric spatter-bearing ignimbrite: the Quaternary Adeje Formation, Cañadas Volcano, Tenerife. *Bull Volcanol* 75:1–15. <https://doi.org/10.1007/s00445-013-0722-5>
- Dias Filho JLE, Xavier GC, Maia PCA, Santos VG (2014) Durability of ornamental gneisses from Pádua-RJ as covering stone. *Electron J Geotech Eng* 21:1957–1976
- Diñer İ, Özvan A, Akin M, Tapan M, Oyan V (2012) İgnimbiritlerin Kapiler su emme potansiyellerinin değerlendirilmesi: Ahlat Taşı Örneği. *J Inst Nat App Sci* 17:64–71
- Durmeková T, Ružička P, Hain M, Čaplovičová M (2015) Changes in marble quality after sodium sulphate crystallization and long-lasting freeze-thaw testing. In: Lollino G, Manconi A, Guzzetti F, Culshaw M, Bobrowsky P, Luino F (eds) *Engineering Geology for Society and Territory* 5:237–241. Springer, Cham. https://doi.org/10.1007/978-3-319-09048-1_46
- Edgar CJ, Wolff JA, Olin PH, Nichols HJ, Pittari A, Cas RAF, Reiners PW, Spell TL, Martí J (2007) The late Quaternary Diego Hernandez Formation, Tenerife: Volcanology of a complex cycle of voluminous explosive phonolitic eruptions. *J Volcanol Geotherm Res* 160:59–85. <https://doi.org/10.1016/j.jvolgeores.2006.06.001>
- Engidasew T (2014) Engineering geological characterization of volcanic rocks of Ethiopian and Sardinian highlands to be used as construction materials. Ph. D. thesis. University of Cagliari, Cagliari Italy.

- Engidasew T, Asmelash A (2016) Assessment and evaluation of volcanic rocks used as construction materials in the city of Addis Ababa. *Momona Ethiop J Sci* 8:193. <https://doi.org/10.4314/mejs.v8i2.7>
- Ersoy H, Karahan M, Babacan AE, Sünnetci MO (2019) A new approach to the effect of sample dimensions and measurement techniques on ultrasonic wave velocity. *Eng Geol* 251:63–70. <https://doi.org/10.1016/j.enggeo.2019.02.011>
- Fort R, Varas MJ, Alvarez de Buergo M, Martín-Freire D (2011) Determination of anisotropy to enhance the durability of natural stone. *J Geophys Eng* 8:132–144. <https://doi.org/10.1088/1742-2132/8/3/S13>
- Franzini M, Leoni L, Lezzerini M, Cardelli R (2007) Relationships between mineralogical composition, water absorption and hydric dilatation in the ‘Macigno’ sandstones from Lunigiana (Massa, Tuscany). *Eur J Mineral* 19:113–123. <https://doi.org/10.1127/0935-1221/2007/0019-0113>
- Freire-Lista DM, Sousa LMO, Carter R, Al-Na’imī F (2021) Petrography and petrophysical characterisation of the heritage stones of Fuwairit Archaeological Site (NW Qatar) and their historical quarries: Implications for heritage conservation. *Episodes* 44:43–58. <https://doi.org/10.18814/epiugs/2020/0200s12>
- Fúster JM, Araña V, Brandle JL, Navarro M, Alonso V, Aparicio A (1968) *Geología y volcanología de las Islas Canarias*. Tenerife. Instituto Lucas Mallada, CSIC. Madrid.
- Germinario L, Siegesmund S, Maritan L, Claudio M (2017) Petrophysical and mechanical properties of Eugeanean trachyte and implications for dimension stone decay and durability performance. *Environ Earth Sci* 76:739–760. <https://doi.org/10.1007/s12665-017-7034-6>
- Ghobadi MH, Babazadeh R (2015) Experimental studies on the effects of cyclic freezing–thawing, salt crystallization, and thermal shock on the physical and mechanical characteristics of selected sandstones. *Rock Mech Rock Eng* 48:1001–1016. <https://doi.org/10.1007/s00603-014-0609-6>
- González de Vallejo LI, Ferrer-Gijón M, Hijazo-Ramiro T (2006) Caracterización geomecánica de los materiales volcánicos de Tenerife. In: Instituto Geológico y Minero de España (IGME) (ed), Madrid, pp 1–147
- Graue B, Siegesmund S, Middendorf B (2011) Quality assessment of replacement stones for the Cologne Cathedral: mineralogical and petrophysical requirements. *Environ Earth Sci* 63:1799–1822. <https://doi.org/10.1007/s12665-011-1077-x>
- Guama-Arico, S.L. (2021) *Trabajos en Piedra Natural*. In: Rodríguez P (ed) *Trabajos en Piedra Natural*, Guama-Arico, S.L., Tenerife, pp 1–56
- Guillou H, Carracedo JC, Paris R, Pérez-Torrado FJ (2004) Implications for the early shield-stage evolution of Tenerife from K/Ar ages and magnetic stratigraphy. *Earth, Planet Sci Lett* 222:599–614. <https://doi.org/10.1016/j.epsl.2004.03.012>
- Hernández-Durán G, Arranz-González JC, de la Vega-Panizo R (2016) Análisis comparativo de propuestas para la ordenación de la actividad extractiva de áridos en la Isla de Tenerife. *Boletín del Instituto Geológico y Minero de España (IGME)* 127:755–773. <https://doi.org/10.21701/bolgeomin.127.4.001>
- Hernández-Gutiérrez LE (2014) Caracterización geomecánica de las rocas volcánicas de las Islas Canarias. Ph. D. thesis. University of La Laguna, La Laguna, Spain.
- Hernández-Gutiérrez LE, Rodríguez-Losada J, Olalla C (2015) Clasificación de litotipos volcánicos altamente cohesivos de las Islas Canarias para su aplicación en ingeniería geológica. In Hernández-Gutiérrez LE, Santamarta J (eds) *Ingeniería geológica en terrenos volcánicos. Métodos, técnicas y experiencias en las Islas Canarias*. Ilustre Colegio Oficial de Geólogos, Madrid, pp 17–34
- IGME. Instituto Geológico y Minero de España (2007). *Continuous Geological Map of Spain Scale 1/50.000*. Ministerio de Ciencia e Innovación. Retrieved (<http://info.igme.es/visorweb/>). Accessed 19 Oct 2021
- IGME. Instituto Geológico y Minero de España (2017). *Plan GEODE de Cartografía Geológica Conintua. Leyenda Descriptiva de La Zona 2913*. Ministerio de Ciencia e Innovación.
- İnce İ (2021) Relationship between capillary water absorption value, capillary water absorption speed, and capillary rise height in pyroclastic rocks. *Mining Metall Explor* 38:841–853. <https://doi.org/10.1007/s42461-020-00354-y>
- İnce İ, Bozdağ A, Barstuğan M, Fener M (2021) Evaluation of the relationship between the physical properties and capillary water absorption values of building stones by regression analysis and artificial neural networks. *J Build Eng* 42:103055. <https://doi.org/10.1016/j.jobe.2021.103055>
- Irvine TN, Baragar WRA (1971) A guide to the chemical classification of the common volcanic rocks. *Can J Earth Sci* 8:523–548. <https://doi.org/10.1139/e71-055>
- Kahraman S, Yeken T (2008) Determination of physical properties of carbonate rocks from P-Wave velocity. *Bull Eng Geol Environ* 67:277–281. <https://doi.org/10.1007/s10064-008-0139-0>
- Karaca Z, Günes-Yılmaz N, Goktan RM (2012) Considerations on the European Standard EN 14157 Test Methods: Abrasion resistance of natural stones Used for flooring in buildings. *Rock Mech Rock Eng* 45:103–111. <https://doi.org/10.1007/s00603-011-0190-1>
- Karakuş A, Akatay M (2013) Determination of basic physical and mechanical properties of basaltic rocks from p-wave velocity. *Nondestruct Test Eval* 28:37–41. <https://doi.org/10.1080/10589759.2013.823606>
- Karaman K, Kaya A, Kesimal A (2015) Effect of the specimen length on ultrasonic P-Wave velocity in some volcanic rocks and limestones. *J African Earth Sci* 112:142–149. <https://doi.org/10.1016/j.jafrearsci.2015.09.017>
- Kecek B, Gokay MK (2009) Mechanical properties of Erciyes Mountain volcanics and their usability as dimensional building stone. In proceeding: 9th International Multidisciplinary Scientific Geconference of Modern Management of Mine Producing, Geology and Environmental Protection. 14–19 Jun, 2009, SGEM, Bulgaria, pp 441–448
- Kılıç A, Teymen A (2008) Determination of mechanical properties of rocks using simple methods. *Bull Eng Geol Environ* 67:237–244. <https://doi.org/10.1007/s10064-008-0128-3>
- Kurtulus C, Bozkurt A, Endes H (2012) Physical and mechanical properties of serpentinized ultrabasic rocks in NW Turkey. *Pure Appl Geophys* 169:1205–1215. <https://doi.org/10.1007/s00024-011-0394-z>
- Larraz-Mora A (1999) La piedra como material de construcción en Tenerife a principios del siglo XVI: Normativa, extracción y tipos. *Revista De Historia Canaria* 181:105–126
- Le Bas MJ, Le Maitre RW, Streckeisen A, Zanettin B (1986) A chemical classification of volcanic rocks based on the total alkali-silica diagram. *J Petrol* 27:745–750. <https://doi.org/10.1093/petrology/27.3.745>
- López-Doncel R, Wedekind W, Aguillón-Robles A, Dohrmann R, Molina-Maldonado S, Leiser T, Wittenborn A, Siegesmund S (2018) Thermal expansion on volcanic tuff rocks used as building stones: examples from Mexico. *Environ Earth Sci* 77:338. <https://doi.org/10.1007/s12665-018-7533-0>
- López-Doncel R, Wedekind W, Dohrmann R, Siegesmund S (2013) Moisture expansion associated to secondary porosity. An example of the Loseros Tuff of Guanajuato, Mexico. *Environ Earth Sci* 69:1189–1201. <https://doi.org/10.1007/s12665-012-1781-1>
- López-Doncel R, Wedekind W, Leiser T, Molina-Maldonado S, Velasco-Sánchez A, Dohrmann R, Kral A, Wittenborn A, Aguillón-Robles A, Siegesmund S (2016) Salt bursting tests on volcanic tuff rocks from Mexico. *Environ Earth Sci* 75:212. <https://doi.org/10.1007/s12665-015-4770-3>

- Mahmutoğlu Y (2017) Prediction of weathering by thermal degradation of a coarse-grained marble using ultrasonic pulse velocity. *Environ Earth Sci* 76:1–20. <https://doi.org/10.1007/s12665-017-6770-y>
- Marrero-Cabrera JL (2000) Introducción. In: Excmo. Ayuntamiento de Arucas, Fundación para la Etnografía y el Desarrollo de la Artesanía Canaria (FEDAC) (eds) *Los Labrantes de Arucas*. Ediciones del Umbral, Las Palmas de Gran Canaria, pp 15–16
- Martínez-Martínez J, Pol A, García-Sánchez L, Reyes-Agustín G, Osorio-Ocampo LS, Macías-Vázquez JL, Robles-Camacho J (2018) Building stones used in the architectural heritage of Morelia (México): Quarries location, rock durability and stone compatibility in the monument. *Environ Earth Sci* 77:1–16. <https://doi.org/10.1007/s12665-018-7340-7>
- Mendoza-Chavez G, Martínez-Martínez LH, Delgado-Hernandez DJ, De León ED, Alonso-Guzmán EM, Martínez-Molina W, Arreygue-Rocha E, Chavez-García HL, Arteaga-Arcos JC (2012) Mechanical properties of rocks used for the construction of vehicular bridges supported by pier masonry. *Adv Mat Res* 535–537:1881–1888. <https://doi.org/10.4028/www.scientific.net/AMR.535-537.1881>
- Molina E, Cultrone G, Sebastián E, Alonso FJ (2013) Evaluation of stone durability using a combination of ultrasound, mechanical and accelerated aging tests. *J Geophys Eng* 10:35003–35021. <https://doi.org/10.1088/1742-2132/10/3/035003>
- Moon K, Park S, Kim Y, Yang S (2014) Mechanical characteristics of basalt in Jeju Island with relation to porosity. *KSCE J Civ Eng* 34:1215–1225. <https://doi.org/10.12652/Ksce.2014.34.4.1215>
- Müller B, Hausmann J, Niedzwiedz H (2009) Prediction and minimisation of vibrations during production blasts. In proceeding: International symposium on rock fragmentation by blasting, 12–13 Sep, 2009, Spain (Granada), pp 47–55.
- Murast S, Hakki-Tarik Ö (2016) The importance of welded tuff stones in construction industry according to their physico-mechanical properties. *HU J Eng* 1:8–18
- Mustafa S, Khan MA, Khan MR, Hameed F, Mughal MS, Asghar A, Niaz A (2015) Geotechnical study of marble, schist, and granite as dimension stone: a case study from parts of Lesser Himalaya, Neelum Valley Area, Azad Kashmir, Pakistan. *Bull Eng Geol Environ* 74:1475–1487. <https://doi.org/10.1007/s10064-015-0719-8>
- Navarro R, Pereira D, Gimeno A, Del Barrio S (2018) Influence of natural carbonation process in serpentinites used as construction and building materials. *Constr Build Mater* 170:537–546. <https://doi.org/10.1016/j.conbuildmat.2018.03.100>
- Novotný M, Skácelová Z, Mrlina J, Mičoch B, Růžek B (2009) Depth-recursive tomography along the eger rift using the S01 profile refraction data: Tested at the KTB super drilling hole, structural interpretation supported by magnetic, gravity and petrophysical data. *Sur Geophys* 30:561–600. <https://doi.org/10.1007/s10712-009-9068-0>
- Oliveira LI (2017) Estudo de um traquito da região de Mafra para aplicação como rocha ornamental. Master's thesis. University of Nova de Lisboa, Lisboa, Portugal.
- Öner F, Türkmen S, Özbek A, Karakaya T (2006) Engineering properties of Hınıs ignimbrites and their usability as a building stone (Erzurum, Turkey). *Environ Geol* 50:275–284. <https://doi.org/10.1007/s00254-006-0208-2>
- Ozcelik Y, Ozguven A (2014) Water absorption and drying features of different natural building stones. *Constr Build Mater* 63:257–270. <https://doi.org/10.1016/j.conbuildmat.2014.04.030>
- Ozguven A, Ozcelik Y (2013) Investigation of some property changes of natural building stones exposed to fire and high heat. *Constr Build Mater* 38:813–821. <https://doi.org/10.1016/j.conbuildmat.2012.09.072>
- Özvan A, Dinger I, Akin M, Oyan V, Tapan M (2015) Experimental studies on ignimbrite and the effect of lichens and capillarity on the deterioration of Seljuk Gravestones. *Eng Geol* 185:81–95. <https://doi.org/10.1016/j.enggeo.2014.12.001>
- Parent T, Domeed N, Sellier A, Mouatt L (2015) Mechanical characterization of limestone from sound velocity Measurement. *Int J Rock Mech Min* 79:149–156. <https://doi.org/10.1016/J.IJRMMS.2015.08.009>
- Perucho-Martínez Á (2018) Comportamiento mecánico de las rocas volcánicas. *Revista Digital Del Cedex* 186:39
- Pola A, Crosta G, Fusi N, Castellanza R (2014) General characterization of the mechanical behaviour of different volcanic rocks with respect to alteration. *Eng Geol* 169:1–13. <https://doi.org/10.1016/j.enggeo.2013.11.011>
- Pola A, Martínez-Martínez J, Macías JL, Fusi N, Crosta G, Garduño-Monroy VH, Núñez-Hurtado JA (2016) Geomechanical characterization of the Miocene Cuitzeo ignimbrites, Michoacán, Central Mexico. *Eng Geol* 214:79–93. <https://doi.org/10.1016/j.enggeo.2016.10.003>
- Pözl C, Siegesmund S, López-Doncel R, Dohrmann R (2022) Key parameters of volcanic tuffs used as building stone: a statistical approach. *Environ Earth Sci* 81:1–29. <https://doi.org/10.1007/s12665-021-10114-w>
- Rahmouni A, Boulanouar A, Boukalouch M, Géraud Y, Samaouali A, Harnafi M, Sebbani J (2013) Prediction of porosity and density of calcarenite rocks from P-wave velocity measurements. *Int J Geosci* 4:1292–1299. <https://doi.org/10.4236/ijg.2013.49124>
- Ribeiro CM (2013) Avaliação do desempenho de revestimentos superficiais na durabilidade de pedra de construção. Master's thesis. University of Minho, Braga, Portugal.
- Rivas T, Prieto B, Silva B (2000) Influence of rift and bedding plane on the physico-mechanical properties of granitic rocks. Implications for the deterioration of granitic monuments. *Build Environ* 35:387–396. [https://doi.org/10.1016/S0360-1323\(99\)00037-2](https://doi.org/10.1016/S0360-1323(99)00037-2)
- Rodríguez-Losada JA, Hernández-Gutiérrez LE, Olalla C, Perucho A, Serrano A, Del Potro R (2007a) The volcanic rocks of the Canary Islands. Geotechnical properties. In proceeding: ISRM International Workshop on Volcanic Rock, 14–15 Jul, 2007, Portugal (Azores), pp 53–57
- Rodríguez-Losada JA, Hernández-Gutiérrez LE, Lomoschitz A (2007b) Geotechnical features of the welded ignimbrites of the Canary Islands. In proceeding: ISRM International Workshop on Volcanic Rock, 14–15 Jul, 2007, Portugal (Azores), pp 29–33
- Rodríguez-Pérez I, Vasconcelos G, Lourenço PB, Quintana P, García C, Dionísio A (2021) Physical-mechanical characterization of limestones from Yucatan churches. Mexico. *J Build Eng* 44:102895. <https://doi.org/10.1016/j.jobe.2021.102895>
- Saldaña M, González J, Pérez-Rey I, Jeldres M, Toro N (2020) Applying statistical analysis and machine learning for modeling the UCS from P-wave velocity, density and porosity on dry travertine. *Appl Sci* 10:4565. <https://doi.org/10.3390/app10134565>
- Santos I, Sousa LMO, Lourenço J (2018) Granite resource evaluation: example of an extraction area in the north of Portugal. *Environ Earth Sci* 77:608. <https://doi.org/10.1007/s12665-018-7780-0>
- Sarıışık G (2020) Investigation of the effect of the environmental interaction characteristics of volcanic rocks on several properties before and after heating processing. *Fresenius Environ Bull* 29:7367–7378
- Sarıışık G, Özkan E, Kundak E, Akdaş H (2016) Classification of parameters affecting impact resistance of natural stones. *J Test Eval* 44:1650–1660. <https://doi.org/10.1520/JTE20140276>
- Sarkar K, Vishal V, Singh TN (2012) An empirical correlation of index geomechanical parameters with the compressional wave velocity. *Geotech Geol Eng* 30:469–479. <https://doi.org/10.1007/s10706-011-9481-2>

- Schaefer LN, Kendrick JE, Oommen T, Lavallée Y, Chigna G (2015) Geomechanical rock properties of a basaltic volcano. *Front Earth Sci* 3:1–15. <https://doi.org/10.3389/feart.2015.00029>
- Schwartz-Mesa C (2016) Petrogenesis and physical volcanology of a compositionally zoned ignimbrite on Tenerife, Canary Islands, Spain. Master's Thesis, University of Leicester.
- Sengun N, Demirdag S, Ugur I, Akbay D, Altindag R (2015) Assessment of the physical and mechanical variations of some travertines depend on the bedding plane orientation under physical weathering conditions. *Constr Build Mater* 98:641–648. <https://doi.org/10.1016/j.conbuildmat.2015.08.142>
- Sharma PK, Khandelwal M, Singh TN (2011) A correlation between Schmidt hammer Rebound numbers with impact strength index, slake durability index and P-wave velocity. *Int J Earth Sci* 100:189–195. <https://doi.org/10.1007/s00531-009-0506-5>
- Siegesmund S, Dürrast H (2014) Physical and mechanical properties of rocks. In: Siegesmund S, Snethlage R (eds) *Stone in architecture*. Springer, Berlin, pp 97–224
- Siegesmund S, Sousa LMO, López-Doncel R (2018) Editorial to the topical collection in *Environmental Earth Sciences* “Stone in the architectural heritage: from quarry to monuments-environment, exploitation, properties and durability.” *Environ Earth Sci* 77:730. <https://doi.org/10.1007/s12665-018-7755-1>
- Siegesmund S, Pözl C, López-Doncel R, Gross CJ, Dohrmann R, Ufer K (2022) Overview and quality assessment of volcanic tuffs in the Mexican building heritage. *Environ Earth Sci* 81:426. <https://doi.org/10.1007/s12665-022-10530-6>
- Silva J, Ferraz E, Gomez C, Casal-Moura A, Grade J (2002) Natural stone from the Madeira Archipelago. Dependence on lithology of Its physico-mechanical behaviour. In proceeding: ISRM International Symposium - EUROCK 2002, 25–27 Nov, 2002, Portugal (Madeira)
- Snethlage R, Pfanner M (2005) Methoden und Laboruntersuchungen zur Konservierung. In: Fraunhofer IRB Verlag (ed) *Leitfaden Steinkonservierung: Planung von Untersuchungen und Maßnahmen zur Erhaltung von Denkmälern aus Naturstein*. Stuttgart.
- Sousa LMO (2014) Petrophysical properties and durability of granites employed as building stone: A comprehensive evaluation. *Bull Eng Geo Environ* 73:569–588. <https://doi.org/10.1007/s10064-013-0553-9>
- Sousa LMO, Suárez del Río LM, Calleja L, Ruiz de Argandoña V, Rodríguez A (2005) Influence of microfractures and porosity on the physico-mechanical properties and weathering of ornamental granites. *Eng Geol* 77:153–168. <https://doi.org/10.1016/j.enggeo.2004.10.001>
- Sousa LMO, Oliveira AS, Alves IMC (2016) Influence of fracture system on the exploitation of building stones: the case of the Mondim de Basto granite (north Portugal). *Environ Earth Sci* 75:39. <https://doi.org/10.1007/s12665-015-4824-6>
- Sousa LMO, Lourenço J, Pereira D (2019) Suitable Re-Use of abandoned quarries for restoration and conservation of the old city of Salamanca - World Heritage Site. *Sustainability* 11:4352. <https://doi.org/10.3390/su11164352>
- Sousa LMO, Menningen J, López-Doncel R, Siegesmund S (2021) Petrophysical properties of limestones: Influence on behaviour under different environmental conditions and applications. *Environ Earth Sci* 80:814. <https://doi.org/10.1007/s12665-021-10064-3>
- Teymen A, Mengüç EC (2020) Comparative evaluation of different statistical tools for the prediction of uniaxial compressive strength of rocks. *Int J Min Sci Techn* 30:785–797. <https://doi.org/10.1016/j.ijmst.2020.06.008>
- Tilley CE (1960) Differentiation of Hawaiian basalts: some variants in lava suites of dated Kilauean eruptions. *J Petrol* 1:47–55. <https://doi.org/10.1093/petrology/1.1.47>
- Tuğrul A, Zarif IH (1999) Correlation of mineralogical and textural characteristics with engineering properties of selected granitic rocks from Turkey. *Eng Geol* 51:303–317. [https://doi.org/10.1016/S0013-7952\(98\)00071-4](https://doi.org/10.1016/S0013-7952(98)00071-4)
- Türkdönmez O, Bozcu M (2012) The geological, petrographical and engineering properties of rhyolitic tuffs (Çan Stone) in Çan-etili area (Çanakkale), NW Turkey: Their usage as building and covering stones. *Open J Geol* 2:25–33. <https://doi.org/10.4236/ojg.2012.21003>
- Ünal M, Altunok E (2019) Determination of water absorption properties of natural building stones and their relation to porosity. *E-J New World Sci Acad* 14:39–45. <https://doi.org/10.12739/NWSA.2019.14.1.1A0429>
- Vanorio T, Prasad M, Patella D, Nur A (2002) Ultrasonic velocity measurements in volcanic rocks: correlation with microtexture. *Geophys J Int* 149:22–36. <https://doi.org/10.1046/j.0956-540x.2001.01580.x>
- Vázquez P, Alonso FJ, Esbert RM, Ordaz J (2010) Ornamental granites: Relationships between p-waves velocity, water capillary absorption and the crack network. *Constr Build Mater* 24:2536–2541. <https://doi.org/10.1016/j.conbuildmat.2010.06.002>
- Vieira F, Cueto N, Pereira M, Santos P (2018) Mechanical and physical properties of volcanic rocks from Madeira Island, Portugal. In: *Proceeding of conference 16° Congresso Nacional de Geotecnia, Azores, Portugal, 27–30 May, 2018*.
- Warr LN (2021) IMA–CNMNC approved mineral symbols. *Mineral Mag* 85:291–320. <https://doi.org/10.1180/mgm.2021.43>
- Wedekind W, Ruedrich J, Siegesmund S (2011) Natural building stones of Mexico–Tenochtitlán: their use, weathering and rock properties at the Templo Mayor, Palace Heras Soto and the Metropolitan Cathedral. *Environ Earth Sci* 63:1787–1798. <https://doi.org/10.1007/s12665-011-1075-z>
- Wedekind W, López-Doncel R, Dohrmann R, Kocher M, Siegesmund S (2013) Weathering of volcanic tuff rocks caused by moisture expansion. *Environ Earth Sci* 69:1203–1224. <https://doi.org/10.1007/s12665-012-2158-1>
- Yagiz S (2010) Geomechanical properties of construction stones quarried in south-western Turkey. *J Sci Res Essay* 5:750–757
- Yagiz S (2011) P-Wave velocity test for assessment of geotechnical properties of some rock materials. *Bull Mater Sci* 34:947–953. <https://doi.org/10.1007/s12034-011-0220-3>
- Yang S-B (2015) Physical and mechanical characteristics of basalts in northwestern and southeastern Jeju Island. *J Korean Geotech Soc* 31:41–52. <https://doi.org/10.7843/kgs.2015.31.7.41>
- Yarahmadi R, Bagherpour R, Khademian A, Sousa LMO, Almasi SN, Esfahani MM (2019) Determining the optimum cutting direction in granite quarries through experimental studies: a case study of a granite quarry. *Bull Eng Geol Env* 78:459–467. <https://doi.org/10.1007/s10064-017-1158-5>
- Yasar E, Tolgay A, Teymen A (2009) Industrial usage of Nevşehir-Kayseri (Turkey) Tuff Stone. *World Appl Sci J* 3:271–284
- Yüksek S (2019) Mechanical properties of some building stones from volcanic deposits of Mount Erciyes (Turkey). *Mater Construcc* 69:187. <https://doi.org/10.3989/mc.2019.04618>
- Yüksek S, Demirci A (2010) Geotechnical properties of volcanic materials of the Mount Erciyes. In proceeding: ISRM International Workshop on Rock Mechanics and Geoenvironment in Volcanic Environments, 31 May–1 Jun, 2010, Spain (Canary Island), pp. 99–105

Publisher's Note Springer Nature remains neutral with regard to jurisdictional claims in published maps and institutional affiliations.